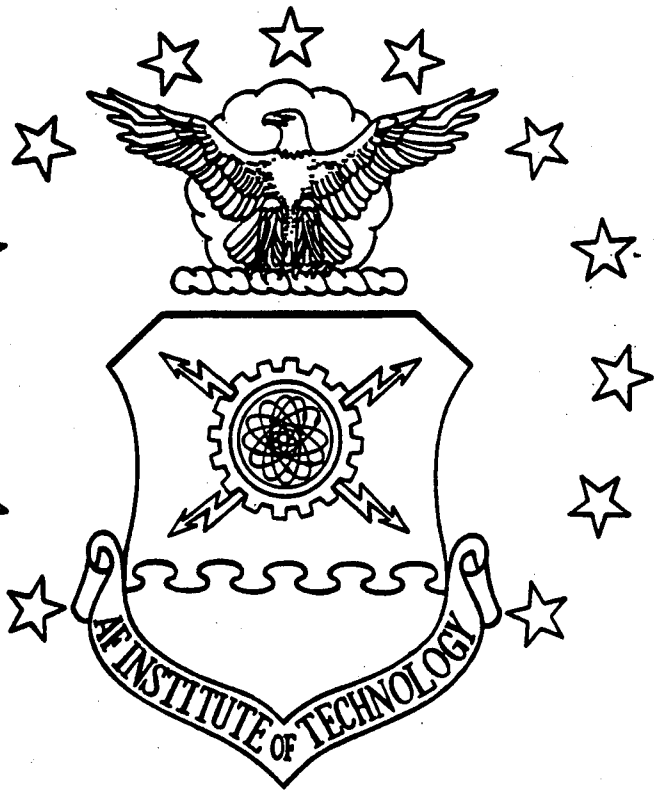

SELECTED
DEC 30 1994
F

19941228 062

Processing of Wide-Angle Synthetic Aperture Radar Signals for Detection of Obscured Ground Targets

THESIS

Richard J. Sumner
Second Lieutenant, USAF

AFIT/GE/ENG/94D-28

This document has been approved for public release and sale; its distribution is unlimited.

DEPARTMENT OF THE AIR FORCE
AIR UNIVERSITY
AIR FORCE INSTITUTE OF TECHNOLOGY

Wright-Patterson Air Force Base, Ohio

AFIT/GE/ENG/94D-28

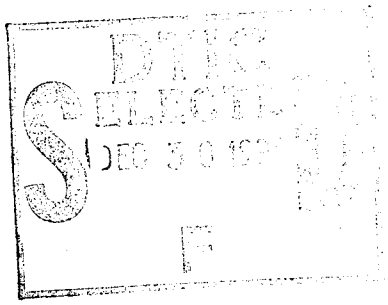

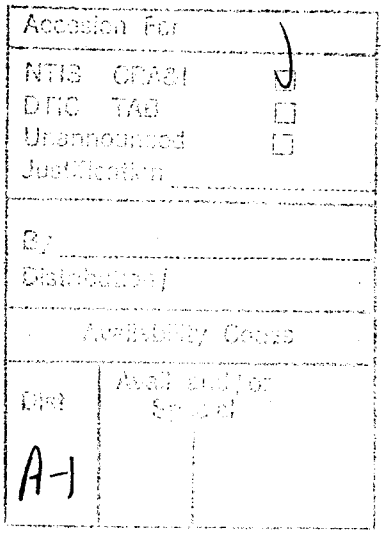

Processing of Wide-Angle Synthetic Aperture Radar Signals for Detection of Obscured Ground Targets

THESIS
Richard J. Sumner
Second Lieutenant, USAF

AFIT/GE/ENG/94D-28

DTIC QUALITY INSPECTED 2

Approved for public release; distribution unlimited

The views expressed in this thesis are those of the author and do not reflect the official policy or position of the Department of Defense or the U. S. Government.

AFIT/GE/ENG/94D-28

Processing of Wide-Angle Synthetic Aperture Radar Signals for Detection of Obscured Ground Targets

THESIS

Presented to the Faculty of the School of Engineering
of the Air Force Institute of Technology
Air University
In Partial Fulfillment of the
Requirements for the Degree of
Master of Science in Electrical Engineering

Richard J. Sumner, BSEE
Second Lieutenant, USAF

December, 1994

Approved for public release; distribution unlimited

Acknowledgements

I would like to thank several people who have made this thesis possible. Dr. Joe Sacchini has been an invaluable source of guidance and information, and his efforts are greatly appreciated. Mrs. Patty Ryan, without whom the data for this thesis would still be in the development and error-correction stage. Loral and Wright Labs Target Recognition Branch (WL/AARA) for making the data available to students on a limited basis, and also to WL/AARA for sponsoring this thesis. To the instructors at AFIT for providing excellent instruction in a down-to-earth manner, and to the United States Air Force for providing this education. To my fellow students Robert Garza, Lori Thorson, Georgia Harrup, Roger Claypoole, Chris Eisenbies, Gerry Falen, Wayne McLaggan, and Jeff Gay. You all made a difficult curriculum bearable and even fun. To my good friends Dennis, Dave, Rob, Brent, Lori, Roger, and Joe. Ya'll made my transition to the yankee way of life as good as it could be, and I won't forget you. Finally, the most thanks belong to my parents, who instilled in me all the values I now hold true and the perseverance to make it through this program.

Richard J. Sumner

Table of Contents

		Page
Acknowledgements		ii
List of Figures		vi
List of Tables		ix
Abstract		x
I.	Introduction	1-1
	1.1 Significance of Problem	1-1
	1.2 Background	1-2
	1.3 Problem	1-4
	1.4 Summary of Chapters	1-7
II.	Image Rotation and Registration	2-1
	2.1 Overview	2-1
	2.2 Background	2-1
	2.2.1 Rotation Methods	2-2
	2.2.2 Performance of Rotation Methods	2-4
	2.3 Ground Plane Transformation	2-6
	2.4 Data Generation	2-7
	2.5 Summary of Chapter	2-11
III.	Image Processing	3-1
	3.1 Overview	3-1
	3.2 WASAR Pre-Processing Methods	3-1
	3.2.1 Display of Images	3-2
	3.2.2 WASAR Pre-Processing Methods	3-3

Page

3.2.3 Mean Method (Mean) 3-3
3.2.4 Subtraction Method (Sub & Sub45) 3-3
3.2.5 Standard Deviation and Variance Methods (SDM & Var) 3-8
3.2.6 Subtraction of Powers Method (SPM) 3-12
3.2.7 Mean of Powers Minus Variance (MPMVM) 3-12
3.3 Statistical Analysis of Various Methods 3-12
3.4 Summary of Chapter 3-17

IV. Target Detection 4-1
4.1 Overview 4-1
4.2 Detection Theory 4-1
4.2.1 Testing of Binary Hypothesis 4-2
4.3 Threshold Detection 4-9
4.4 Detection Performance of WASAR Pre-Processing Methods . 4-10
4.5 Summary of Chapter 4-16

V. Findings and Conclusions 5-1
5.1 Results of Research 5-1
5.2 Recommendations 5-2
5.3 Conclusions 5-4

Appendix A. Computer Routines A-1
A.1 Rotation of Images A-1
A.1.1 Nearest Neighbor Method A-1
A.1.2 Interpolation Method A-2
A.2 Elevation Angle Correction A-4
A.3 Detection A-5
A.3.1 Maximum-Minimum Threshold Setting A-5
A.3.2 Standard Deviations Above Mean Setting A-5

Page

Bibliography BIB-1

Vita VITA-1

List of Figures

Figure		Page
1.1.	SAR Image Formation	1-2
1.2.	WASAR Image Formation	1-3
1.3.	Radar Return from M35 Truck	1-6
2.1.	Overlap of Rotated Image	2-2
2.2.	Simple Test Image for Rotation	2-3
2.3.	Simple Test Image After Nearest Neighbor Rotation	2-3
2.4.	Simple Test Image After Interpolated Rotation	2-4
2.5.	Correlation of Original Image and (a) Nearest-Neighbor Rotated Image, (b) Interpolated Rotated Image	2-5
2.6.	Example of Elevation Angle Distortion	2-6
2.7.	Image of (a) T-72 from a 40° Elevation Angle, 60° Azimuth Angle, (b) Distorted T-72 Due to Elevation Angle, (c) T-72 at 60° Azimuth Angle After Correcting for Elevation Angle, and (d) T-72 After Correcting for Elevation Angle, Rotated from 60° to 0°	2-7
2.8.	Data Set 1 Before Rotation	2-9
2.9.	Data Set 1 After Rotation	2-10
2.10.	(a) Enlarged View of 0° aspect angle, HH Polarization, Data Set 1, (b) Ground Target Map of 0°	2-11
2.11.	Data Set 2 Before Rotation	2-12
2.12.	Data Set 2 After Rotation	2-13
2.13.	(a) Enlarged View of 0° aspect angle, HH Polarization, Data Set 2, (b) Ground Truth Map of 0°	2-14
2.14.	Ground Truth Map Symbol for M-35 Truck	2-14
3.1.	Unprocessed Data (a) Data Set 1, Display 1; (b) Data Set 1, Display 2; (c) Data Set 2, Display 1; and (d) Data Set 2, Display 2	3-4

Figure Page

3.2. Data Processed by Mean Method (a) Data Set 1, Display 1; (b) Data Set 1, Display 2; (c) Data Set 2, Display 1; and (d) Data Set 2, Display 2 . 3-5

3.3. Data Processed by Subtraction Method (a) Data Set 1, Display 1; (b) Data Set 1, Display 2; (c) Data Set 2, Display 1; and (d) Data Set 2, Display 2 3-7

3.4. Data Processed by 45° Subtraction Method (a) Data Set 1, Display 1; (b) Data Set 1, Display 2; (c) Data Set 2, Display 1; and (d) Data Set 2, Display 2 3-9

3.5. Data Processed by Standard Deviation Method (a) Data Set 1, Display 1; (b) Data Set 1, Display 2; (c) Data Set 2, Display 1; and (d) Data Set 2, Display 2 3-10

3.6. Data Processed by Variance Method (a) Data Set 1, Display 1; (b) Data Set 1, Display 2; (c) Data Set 2, Display 1; and (d) Data Set 2, Display 2 3-11

3.7. Data Processed by Subtraction of Powers Method (a) Data Set 1, Display 1; (b) Data Set 1, Display 2; (c) Data Set 2, Display 1; and (d) Data Set 2, Display 2 3-13

3.8. Data Processed by Mean of Powers Minus Variance Method (a) Data Set 1, Display 1; (b) Data Set 1, Display 2; (c) Data Set 2, Display 1; and (d) Data Set 2, Display 2 3-14

4.1. Example of Probability of False Alarm (P_{fa}) 4-3

4.2. Correlation Between True Histogram and Normalized Histogram Meant to Approximate the Probability Mass Function of the same Data (a) Histogram of SAR (0°) and (b) Normalized and Truncated Histogram of Same Data 4-4

4.3. Histograms (Approximate PMFs) of Processed Data, Data Set 1 (Difference in area under PMFs is due to differing histogram bin spacing) . . 4-5

4.4. Histograms (Approximate PMFs) of Processed Data, Data Set 2 (Difference in area under PMFs is due to differing histogram bin spacing) . . 4-6

4.5. Receiver Operating Characteristics, Data Set 1 4-7

4.6. Receiver Operating Characteristics, Data Set 2 4-8

Figure Page

4.7. Performance of Various WASAR Detection Methods, Data Set 1. The line at 8 Detections on the vertical indicate there are 8 known targets. The threshold is set as described earlier as a percentage of the maximum pixel value. 4-12

4.8. Performance of Various WASAR Detection Methods, Data Set 2. The line at 6 Detections on the vertical indicate there are 6 known targets. The threshold is set as described earlier as a percentage of the maximum pixel value. 4-13

4.9. Correlation Between Histograms and Performance Graphs of the Unprocessed Data (Data Set 1, 0^o, HH, SAR (a) Performance of SAR, (b) Histogram of SAR (0^o), (c) Histogram of Clutter Data, and (d) Histogram of Target Data 4-15

List of Tables

Table		Page
3.1.	Statistics of Various Methods, Data Set 1	3-16
3.2.	Statistics of Various Methods, Data Set 2	3-16
4.1.	Performance of Various Methods, Data Set 2 (N/A signifies data not available)	4-14

Abstract

This thesis investigates advanced processing techniques for the detection of radar targets in the presence of clutter. It is assumed that the radar data available consist of multi-aspect angle, fully polarimetric Synthetic Aperture Radar (SAR) images. Various techniques are introduced and tested on available SAR data. These techniques attempt to exploit the multi-aspect angles in order to extract target characteristics not available in any single image. SAR images are manipulated in such a way to decrease the probability of false alarms in the target detection process. Target detection performance of the techniques is presented and compared. The techniques are shown to give superior results than that of regular SAR.

Processing of Wide-Angle Synthetic Aperture Radar Signals for Detection of Obscured Ground Targets

I. Introduction

1.1 Significance of Problem

The detection and identification of military targets is a high priority mission of the Air Force for the purpose of reconnasaince and bombardment. The detection of highly obscured stationary ground targets is an ongoing problem since such targets are much harder to detect than airborne targets. Ground targets are obscured by the radar return from the ground, nearby foliage, and landscape. Airborne targets are relatively easy to detect since any energy not incident to the target is lost to the radar, therefore helping to eliminate false returns. Ground targets are surrounded by radar energy returning objects and features, obscuring the target signature with seemingly random noise. More advanced processing techniques would allow the detection of such targets with common surveillance and radar systems. By using all of the data available about a target such as fully-polarized Synthetic Aperture Radar (SAR) image [6, 9] and multiple aspect-angle views, new detection methods and algorithms could be developed in order to improve detection capabilities. This thesis takes a continuing look at improving the probability of detecting obscured ground targets.

1.2 Background

Before beginning to talk about image processing and detection algorithms, it may be useful to discuss several terms used in this thesis. A key instrument used in target detection is the Synthetic Aperture Radar (SAR). SAR produces high resolution images of a scene of interest. SAR illuminates small "cells" of a scene with an electromagnetic field and records the intensity of the returned field (see Figure 1.1). The resolution of

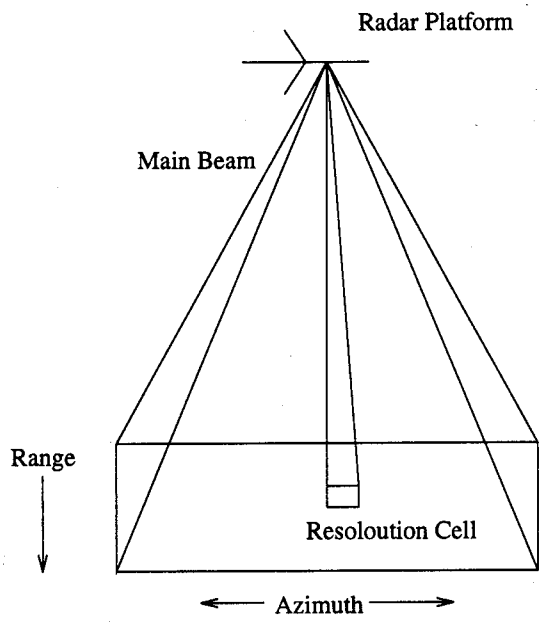

Figure 1.1 SAR Image Formation

the cell is determined by the pulse width of the radar (range resolution) and the distance the radar platform travels (aspect resolution) [1]. All the cells are put together to form a radar image. The drawback to SAR is that only one view of the scene is produced. Thus, if a target is not visible from that angle, either before or after processing, detection is not possible.

Wide-Angle SAR (WASAR) improves SAR by offering several view angles of a target scene. As the radar platform passes the scene of interest, it takes SAR images at several angles (see Figure 1.2). It is believed that a target missed in one view can be detected in another view, or in some optimal combination of several views. Currently, there are no

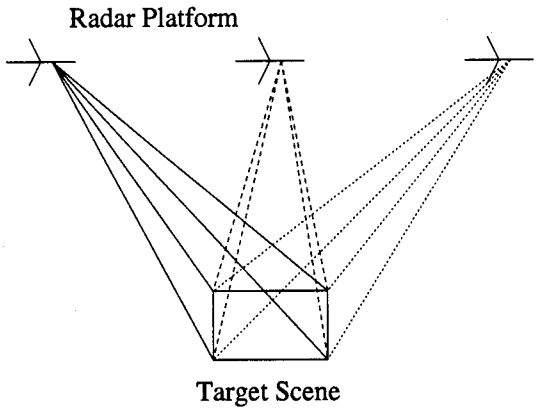

Figure 1.2 WASAR Image Formation

systems or algorithms in common use exploiting the possible advantages of WASAR. This is due to the fact that WASAR for the purpose of detecting ground targets is fairly new technology. However, the use of WASAR is being explored by several groups, such as the Air Force's Wright Laboratories at Wright-Patterson Air Force Base, Ohio. This thesis is an attempt to prove the concept that WASAR is a viable and useful tool.

Several problems arise with the use of WASAR. One problem is that in order to combine the images and perform various algorithms, the images need to be perfectly registered. Perfect registration means that a target at a certain coordinate of an image is at the same coordinate in all images [2]. This presents a problem since it would be difficult for an aircraft to fly in the perfect path to keep the images properly registered, especially in a

combat environment. Another solution is to register the images through signal processing. With accurate knowledge of the aircraft's position and orientation, computer routines can be employed to correctly register the images. Fortunately, the data generated by Wright Labs used in this thesis are initially registered. Another problem of WASAR is that the multiple-aspect angles must be rotated to the same angle before using an algorithm that combines the images. Rotation of the data is a key part of this thesis, and will be discussed more extensively in Chapter II.

Fully polarimetric SAR also improves on SAR by providing more information. Three images are formed of a scene, one with a vertically polarized incident field and vertically polarized receive antenna (VV), one with horizontally polarized incident field and horizontally polarized receive antenna (HH), and one with vertically polarized incident field and horizontally polarized receive antenna (HV). VH (vertical transmitted field, horizontally received) polarization is not used because, due to reciprocity, the VH return is identical to HV [6, 9]. With the use of fully polarimetric radar data, it is believed that targets missed at one polarization may be detected at another. Another use of the multitude of images is that the images can be combined through algorithms designed to reduce the background noise. The combination of Full Polarization and Wide-Angle SAR can provide many times the information gained by standard SAR.

1.3 Problem

The detection of targets in the presence of high intensity clutter is addressed by exploiting multiple view angles made available by WASAR. Clutter is information returned by the scene that is not useful in detection [4]. All data and target information

gained from WASAR is used to improve the probability of detection for obscured targets. The improvements come through the use of new algorithms to extract target signatures available only in separate images. By exploiting the many images that can be formed with radar data, new detection schemes and algorithms are developed in order to better detect the presence of targets. There has been a fair amount of effort recently to improve detection by exploiting characteristics of fully-polarimetric radar data, but little devoted to exploiting WASAR. Novak [8, 7] developed several algorithms designed to reduce the high-frequency speckle of SAR data by combinations of the different polarizations. Speckle is defined as high frequency intensity changes from pixel to pixel. Novak's work succeded in reducing the speckle, but in doing so he had to combine the different polarimetric images without exploiting the differences in them. Knurr [3] worked on using Novak's polarimetric algorithms along with the various angle images from WASAR to improve detection characteristics. The research performed by Knurr only began exploring methods to exploit changes in targets in the various images. It is from Knurr's research that this research begins.

The scope of this thesis is limited to improving the probability of detection of ground targets. Specifically, algorithms are developed to combine all data gathered to improve target detection performance. As the information available about the target increases due to WASAR, detection becomes an easier task. It should be stated that this thesis does not deal with the identification of targets. It only covers improving the probability of correctly deciding if a man-made target is present or not. Since the target is of unknown dimension, the signatures must be assumed to be somewhat abstract. A major, but valid, assumption of this research is that while man made targets tend to change significantly depending on

the angle from which they are viewed, trees and natural objects do not [10]. Figure 1.3

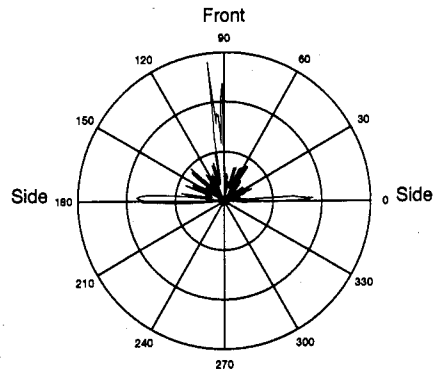

Figure 1.3 Radar Return from M35 Truck

shows how a particular man-made object varies with view angle. The object in question is a $\frac{1}{16}$ scale model of an M35 truck, taken at 0^o elevation and with HH polarization. It shows the radar return (scattered field magnitude) of the truck from one side, around the front, to the other side. The assumption that man-made targets change with angle is an important one. The argument that multiple-angle views of a scene will yield new information on the target depends on little or no new information being gained about the surroundings.

Several things can be done to expand and improve on the body of knowledge currently available. It is known that Novak's speckle reduction algorithms reduce unwanted noise, but they may also be wasting important data by averaging out certain characteristics of the targets. Knurr's [3] work involved using Novak's speckle reduction algorithms [8] and then trying to exploit the multiple angles of WASAR. Knurr developed an algorithm for rotating the WASAR images to a single aspect angle. This rotation is of great importance to the research, since the scene must be rotated properly without losing information.

Since the SAR gathers discrete rather than continuous data sets, proper interpolation of data points is required in order to have the data in a usable form. After a good rotation scheme is implemented, algorithms are employed to extract the changes with respect to the target in the different views. These algorithms exploit the differences in target returns from image to image. The main characteristic exploited is that noise and clutter remain the same while man made objects give returns with large differences from image to image. Several algorithms, called WASAR Pre-Prossessing Algorithms, are developed to exploit this information. One such algorithm is to subtract the images from one another, eliminating the clutter that is of the same magnitude, and enhancing the target return which has a magnitude that changes in each image. Another algorithm developed uses statistical changes from image to image. This seems promising since with changes in aspect angle, the variance of the target is expected to change more that the surroundings. These algorithms are tested and compared to show that detection can be improved with the additional information provided by WASAR.

1.4 Summary of Chapters

Chapter II deals with the rotation of images taken at different angles to the same azimuth angle. Problems resulting from data being taken at an elevation angle are also discussed. Chapter III covers the WASAR Pre-Processing methods used to improve detection performance. Each method is defined and compared visually and statistically. Chapter IV covers target detection, and finally, Chapter V discusses the conclusions and results reached, as well as recommendations for future work.

II. Image Rotation and Registration

2.1 Overview

In this chapter, algorithms for rotating the images are discussed and compared. Specifically, two methods are evaluated for accuracy and efficiency. Problems with image rotation, such as down-sizing and data loss, are discussed. The need for a method to ensure all data are in the ground plane before rotation is discussed and demonstrated, and finally, the two data sets used in this thesis are rotated and compared.

2.2 Background

Before any processing and detection algorithms are performed and evaluated, all images must be transformed into the same coordinate system. Techniques have been developed in the past [3], and a new technique is developed in this thesis to try to improve performance. There are several problems to be addressed when trying to rotate images. First, when turning the images, parts of the new image do not overlap with data from the old image. So the new image can only be as large as the data overlapping the old image. This problem still exists with the method employed in this thesis. The data sets used in this thesis are 512×512 pixel images, and in the worst case (rotation angle = $45°$), the overlap region is 363×363 pixels (Figure 2.1). This down-sizing of the image is necessary in order to keep the data as accurate as possible. Alternatives to size reduction are to either extrapolate the missing data (understandably difficult), or to use a circular image. The processing algorithms used in this thesis are written almost exclusively in Matlab, which is rectangular matrix oriented. It is for this reason that the smaller square images

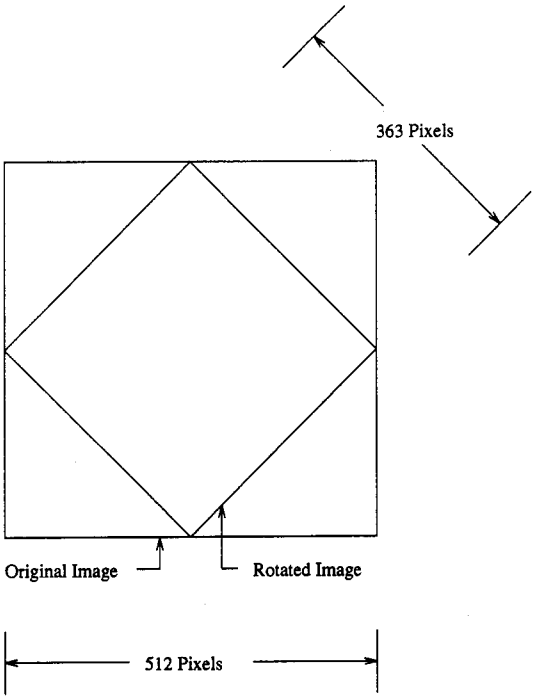

Figure 2.1 Overlap of Rotated Image

are used. Another problem with rotating images is that information is necessarily lost. This is due to the fact that the images are discrete points, and information originally in between the samples is not available for use in rotating the images. The discrete data presents a problem since in turning images, the data between points is often needed for points in the rotated image.

2.2.1 Rotation Methods. At first, a simple routine is used to rotate the image using a nearest neighbor technique. The angle of rotation and the distance from the origin required are used to find the pixel corresponding to the (i,j) coordinates of the pixel in the original image. The images are referenced by the common (row, column) notation, with (1,1) being the upper left hand pixel. Since the image is discrete, the pixels locations are rounded off to the nearest integers, hence the name nearest neighbor. The code for this can

be seen in Appendix A in the Matlab function rotation.m. An example of how information is lost using a nearest neighbor technique can be seen in the rotation of the simple test pattern in Figure 2.2. The image is first turned 45°, then turned 45° back to the original

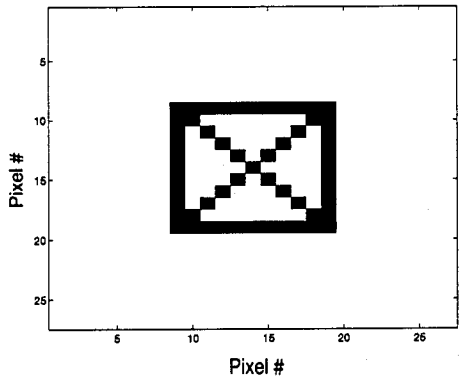

Figure 2.2 Simple Test Image for Rotation

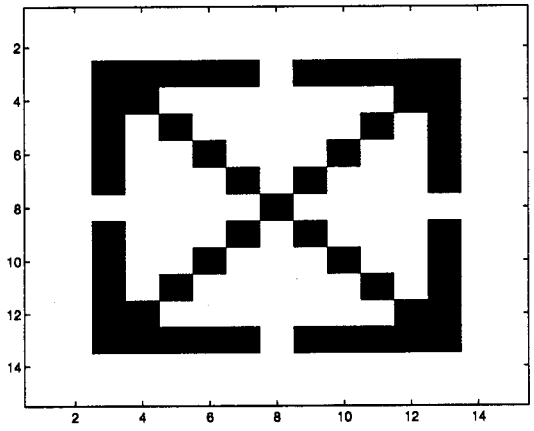

Figure 2.3 Simple Test Image After Nearest Neighbor Rotation

orientation, and the result is shown in Figure 2.3. Figure 2.3 shows that some of the information is lost, most probably due to rounding errors when determining the nearest neighbor. These figures also demonstrate the loss of information that occurs during the rotation process. Another algorithm developed to help eliminate loss of information due to rounding error uses 2-D interpolation. The Matlab code for this function is found in

Appendix A under elcorr2.m. The algorithm interpolates by a given number in between each row of an image, and then does the same to each column. Figure 2.4 shows that all

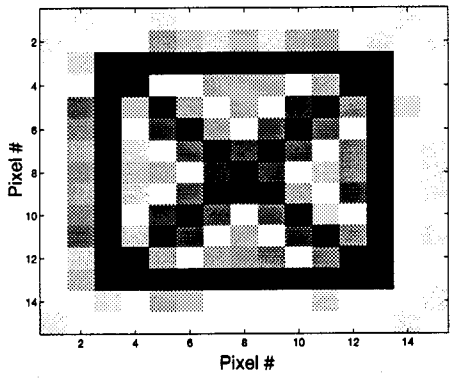

Figure 2.4 Simple Test Image After Interpolated Rotation

the original information is still present. However, interpolation acts as a low-pass filter, and some "smearing" is evident.

2.2.2 Performance of Rotation Methods. As a metric of how each method performs, the 2-D correlation of each method is computed with respect to the original image. When two images are correlated with one another, higher values mean the images are closer to being the same. So an image correlated with itself would have a higher correlation (normalized value of 1.0) than an image correlated with a slightly different one (normalized value less than 1). The interpolated image is slightly more correlated (max normalized value = 0.9481) than the nearest-neighbor method (max normalized value = 0.9298), as can be seen in Figure 2.5.

Another metric worth considering is the relative error, defined as the Frobenius norm of the original image (X_o) minus the rotated image (X_i), divided by the Frobenius norm

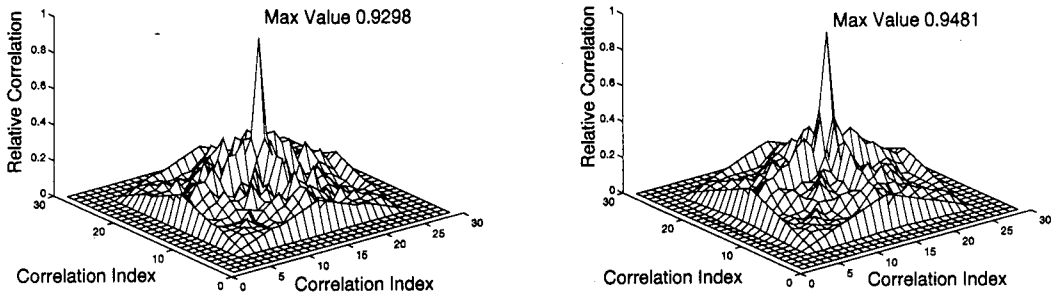

(a) (b)

Figure 2.5 Correlation of Original Image and (a) Nearest-Neighbor Rotated Image, (b) Interpolated Rotated Image

of the original image, or

$$\text{relative error} = \frac{||X_o - X_i||_f}{||X_o||_f}, \tag{2.1}$$

where $||X||_f$ is the Frobenius norm of the matrix X and defined as

$$||X||_f = \sqrt{\sum_{\forall i,j} |X(i,j)|^2}. \tag{2.2}$$

Using this metric, the relative error for the nearest-neighbor method is 0.2649, while for the interpolation method it is 0.2820. This metric indicates the first method is the superior one. Since the results support neither method conclusively, the more efficient nearest-neighbor method was chosen. The second method, in general, should be more accurate, but computationally is too costly. Thus, the first method, the nearest neighbor method, was chosen to rotate all the images in this thesis.

2.3 *Ground Plane Transformation*

Another issue that must be addressed when trying to combine images at different angles is that the images must all lie in the ground plane so distances in one image are correlated with distances in others. If the images are not in the same ground plane, distortions are introduced to the rotated images. This is due to the apparent change in lengths when the elevation angle is changed, as demonstrated in Figure 2.6. This figure

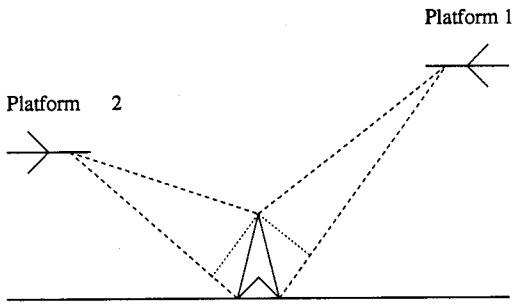

Figure 2.6 Example of Elevation Angle Distortion

shows two radar systems imaging the same object, but at different elevation angles. It is apparent that the object will appear longer to the second radar than to the first. An example of this distortion on a real image can be seen in Figure 2.7. Figure 2.7 (a) shows a T-72 viewed from a 40° elevation angle and a 60° azimuth angle. The tank looks normal, but is viewed from some elevated angle. After rotating the image 60° it is clearly distorted, as seen in Figure 2.7 (b). Thus, to avoid distortion, it is required that the images be in the ground plane before rotation. Figure 2.7 (c) shows the tank image seen in Figure 2.7 (a) after it has been placed in the ground plane. After rotating the corrected image, it looks rectangular, as can be seen in Figure 2.7 (d).

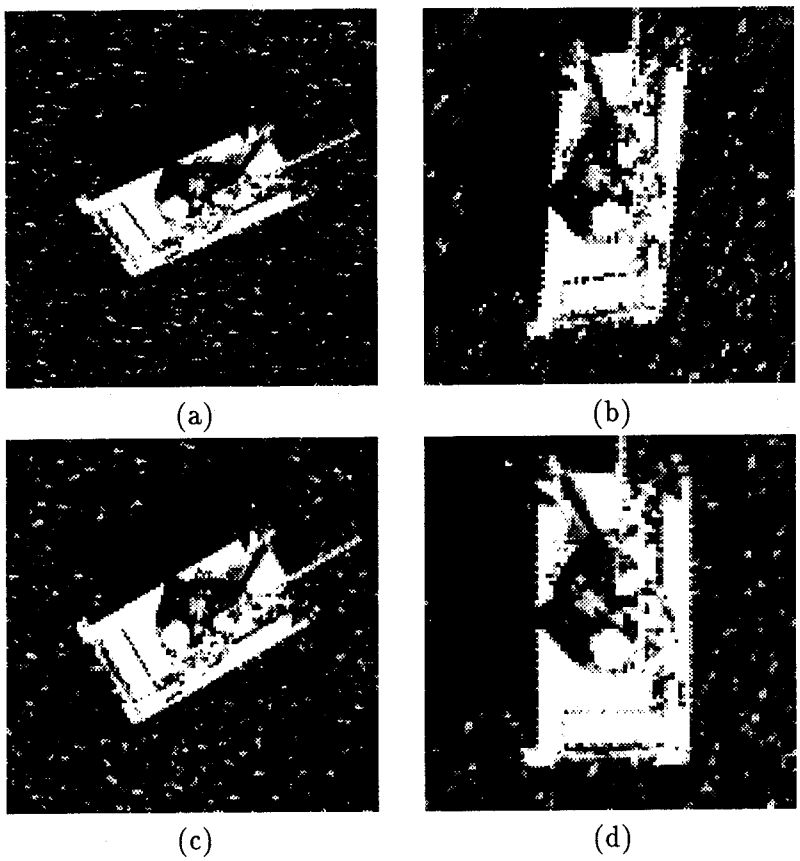

Figure 2.7 Image of (a) T-72 from a 40° Elevation Angle, 60° Azimuth Angle, (b) Distorted T-72 Due to Elevation Angle, (c) T-72 at 60° Azimuth Angle After Correcting for Elevation Angle, and (d) T-72 After Correcting for Elevation Angle, Rotated from 60° to 0°

2.4 Data Generation

The two data sets for this thesis were generated using a pre-release version of software being developed by Loral for the Wright-Labs Target Recognition Branch. The first set consisted of Loral SAR images generated early in the development of the software. At that time, many features were not available. It was chosen because it was the primary data set for an earlier thesis [3], allowing comparisons to be made. The second data set (Data Set 2) consisted of images produced after many revisions of the software, and consequently

is easier to use. Data Set 2 was generated with more realistic target characteristics and statistics. Using this software, images of two scenes were produced for seven different view angles and three polarizations, for a total of 21 images in each data set. The seven aspect angles ranged from -45^o to 45^o in 15^o degree increments. A SAR image at an aspect angle of 45^o refers to an image generated from a swath of data whose center angle corresponds to a radar target orientation of 45^o. Also, all data are magnitudes, with phase information being rejected. This was done since none of the pre-processing algorithms described in the following chapter use phase information. The pixel intensities in the original data ranged numerically from 0 to approximately 120. The pixel intensities reflect the average amount of signal (voltage) returned from the corresponding position in the image. However, the data were normalized to have a unit mean in order to have all information weighted equally in the processing algorithms.

Another major assumption of this thesis is that the data used is a valid representation of radar data from an actual target scene. The Loral code that generates the target scenes has not yet been validated, but the absence of actual WASAR data necessitates the use of the non-validated code.

The raw data from Data Set 1 is seen in Figure 2.8. Figure 2.9 shows Data Set 1 after being rotated using the nearest neighbor method. A better view of the target scene is seen in Figure 2.10 (a), where the known targets are marked with an "$*$". The wide range of values makes the marked targets difficult to see, so Figure 2.10 (b) shows the locations of the targets without the actual image.

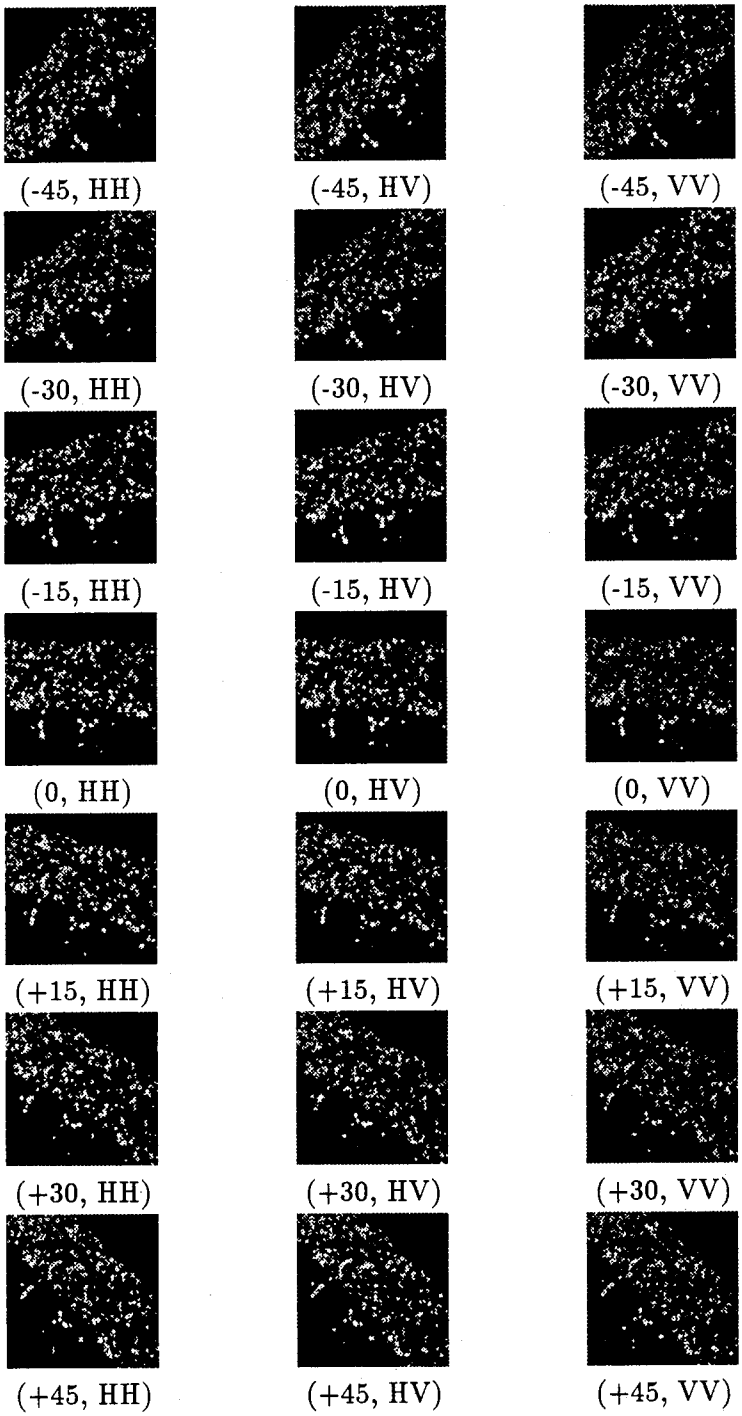

Figure 2.8 Data Set 1 Before Rotation

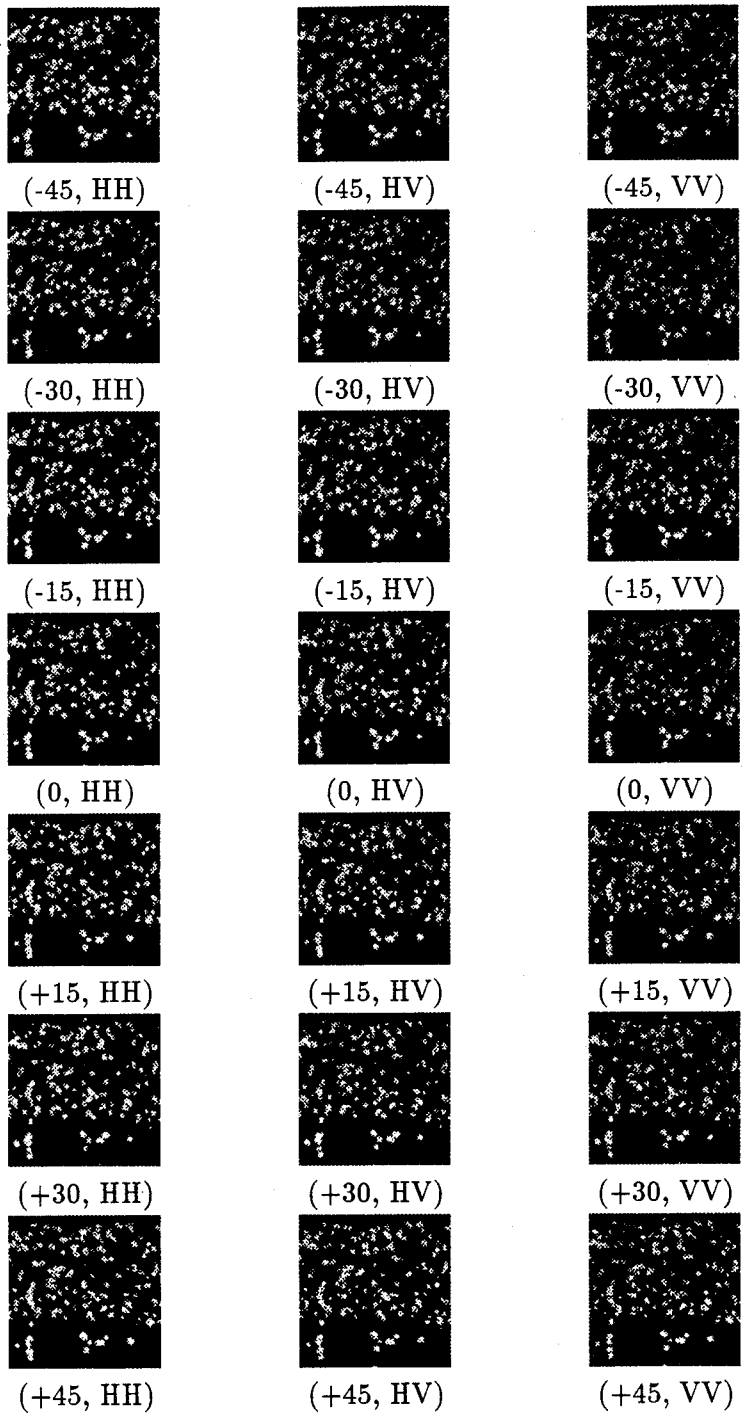

Figure 2.9 Data Set 1 After Rotation

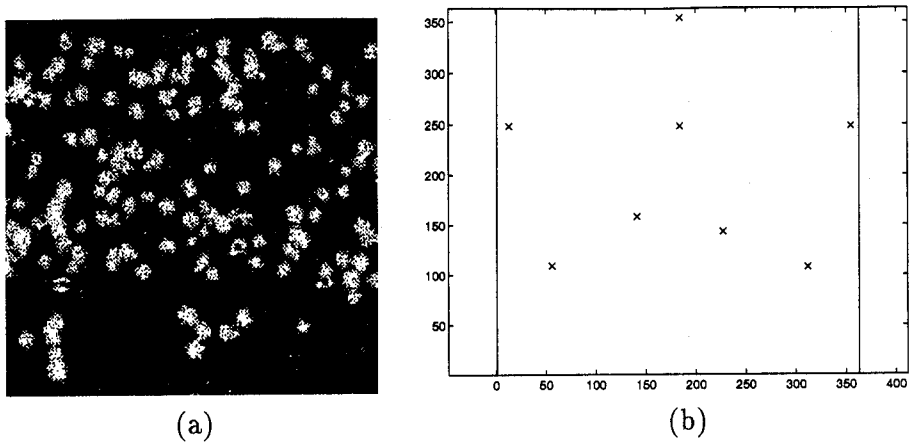

(a) (b)

Figure 2.10 (a) Enlarged View of 0° aspect angle, HH Polarization, Data Set 1, (b) Ground Target Map of 0°

The raw data from Data Set 2 is seen in Figure 2.11. Figure 2.12 shows Data Set 2 after rotation, again with the nearest neighbor method. A better view of one of the images in the Data Set 2 (0°, HH polarization) is seen in Figure 2.13 (a). This figure is also marked with a "*" at the target locations. The ground truth map of Data Set 2 is seen in Figure 2.13 (b). The M-35 truck locations are marked with symbols as in Figure 2.14, the circles are trees, and the lines are ground contours and roads. This map is a new feature of the software, and makes locating targets with respect to trees easier than before.

2.5 Summary of Chapter

This chapter deals with the rotation of images and the associated problems. The performance of the two rotation methods is then discussed. Rotation errors caused by elevation angle, and how to correct for the errors, are also discussed. The elevation error problem is then demonstrated. The generation of Data Sets 1 & 2 is discussed, and the

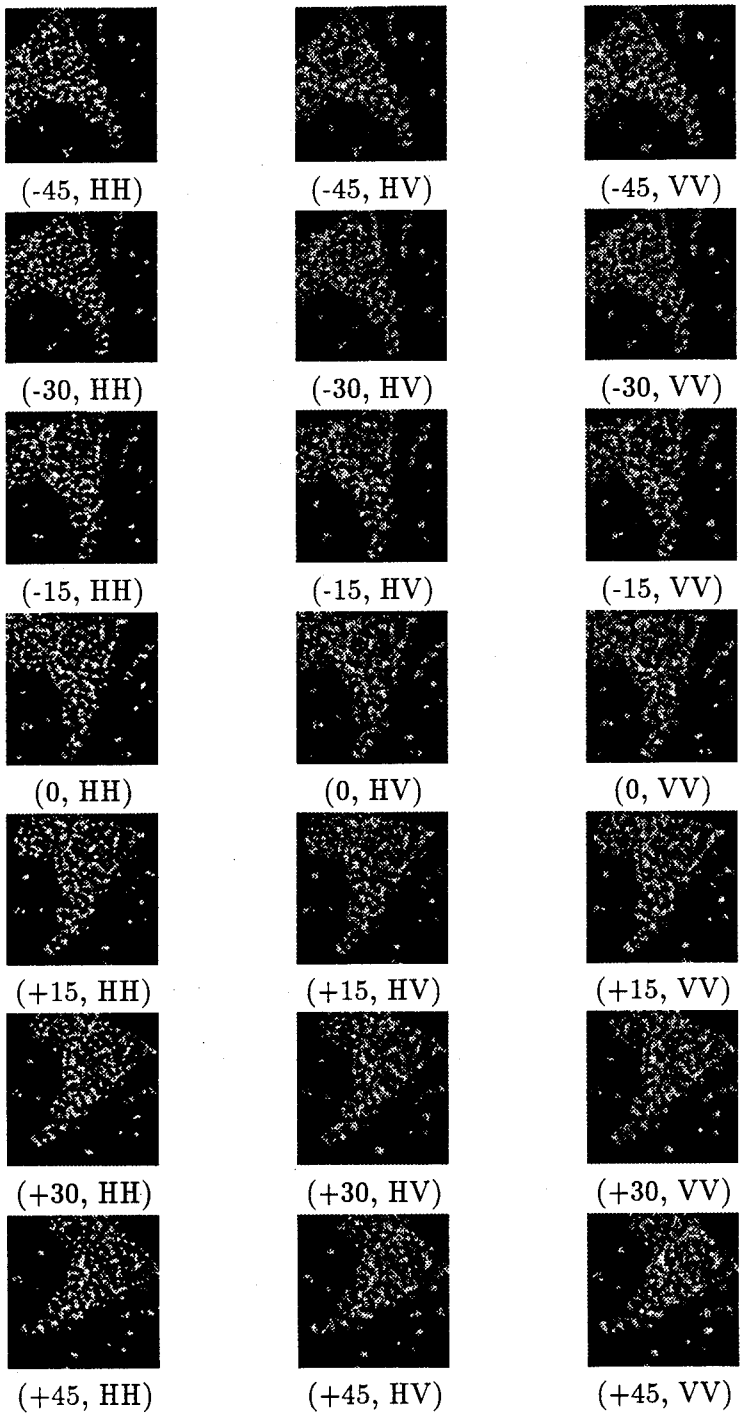

Figure 2.11 Data Set 2 Before Rotation

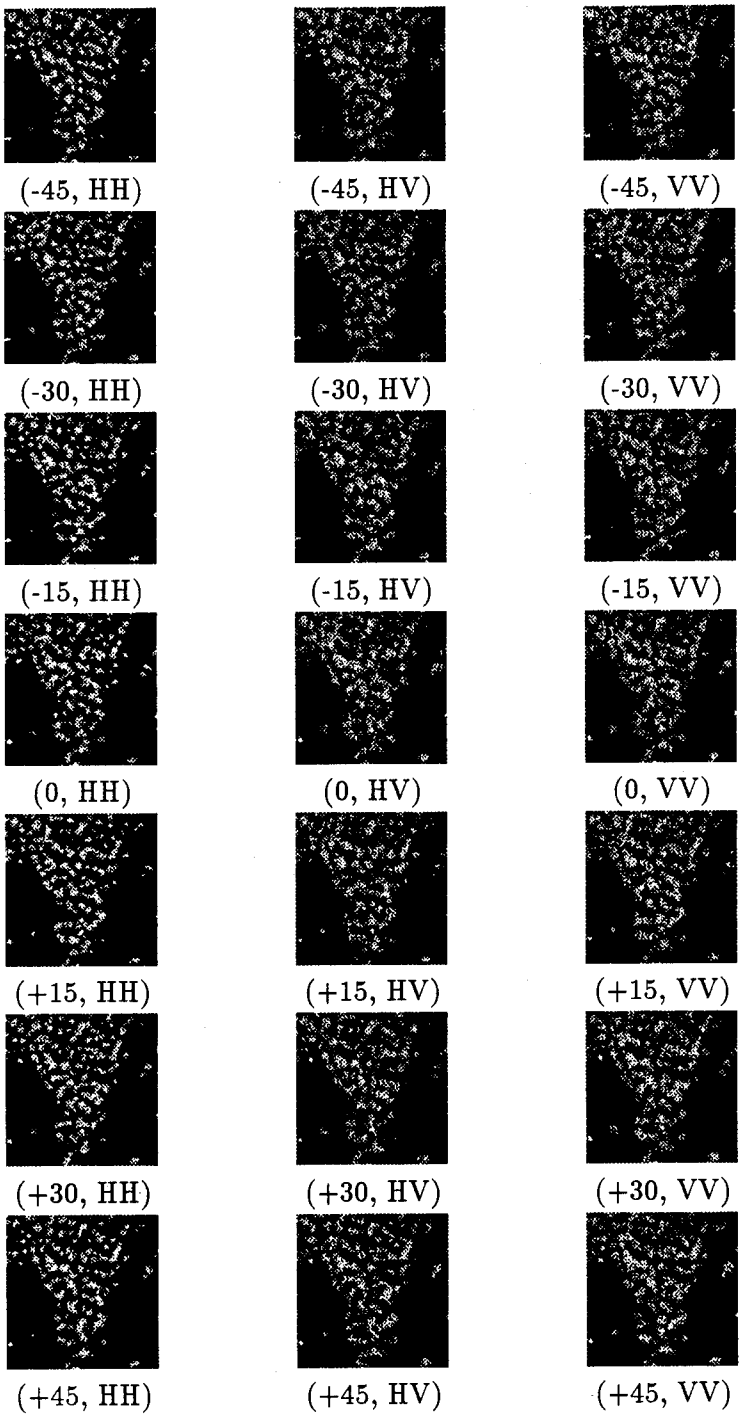

Figure 2.12 Data Set 2 After Rotation

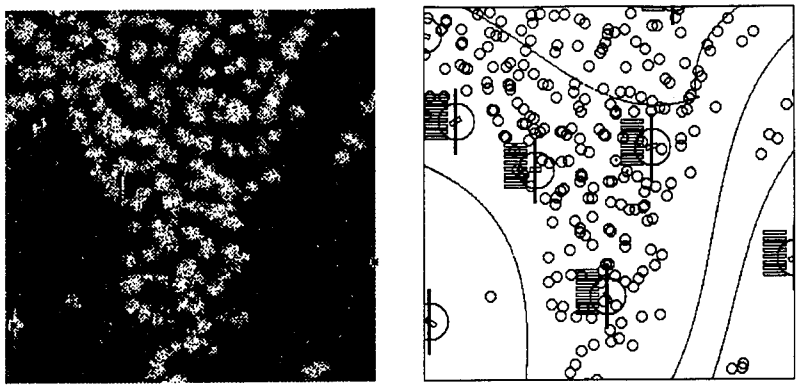

(a) (b)

Figure 2.13 (a) Enlarged View of 0^o aspect angle, HH Polarization, Data Set 2, (b) Ground Truth Map of 0^o

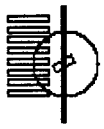

Figure 2.14 Ground Truth Map Symbol for M-35 Truck

various images available in the data sets are provided. The data sets are then shown in the original state and after rotation.

III. Image Processing

3.1 Overview

In this chapter various image processing methods for improving target detection characteristics are discussed. The methods are described in detail, and then implemented on Data Sets 1 and 2. Finally, various statistics of the processed data are given and discussed to show results of the processing. No actual target detection is performed in this chapter, only pre-processing methods to enhance detection characteristics. Target detection is discussed in Chapter IV.

3.2 WASAR Pre-Processing Methods

Recall that the main purpose of this thesis is to improve target detection capabilities. Several methods are devised in order to accomplish this. The following methods are implemented on HH polarized data from each set, with images taken from the seven aspect angles. Since none of the methods use phase information, the phase information is eliminated by taking the magnitude of each pixel in the image. The data are also normalized in order to have all data weighted equally. It should be noted that in these methods the random variables are the pixels from image to image, not pixels within the same image. For example, if an image is formed by subtracting one image from another, the pixel value in the first row and column of the first image is subtracted from the pixel value in the first row and column of the second image, and the result is the pixel value of the resultant image. An example of a random variable is the pixel in the first row and column of each

image. Thus $X_i(1,1)$ is the first realization of a random variable with seven realizations. Each image is a discrete sample of 512 × 512 random variables.

3.2.1 Display of Images. After defining each method, a sample processed image is displayed using two methods. Both remove information from the images in order for the image to look "good" to the human eye. Matlab's image function takes a matrix as an input, and displays each element as a pixel in an image. The displayed pixels range in intensity depending on the corresponding elements value. Elements with a value of zero appear black in the displayed image, and elements with a value of 100 appear white. Elements with values in between 0 and 100 are displayed as shades of gray, and if the elements value is outside this range of values, it is truncated. For example, a value of 101 is displayed as a 100 level element, and -5 is displayed as 0. This characteristic of the image function is used to truncate the data not needed to display the image for the human eye. In some of the images, an outlier may be many standard deviations above the mean. If the image is normalized to range from 0 to 100, most of the image would appear black due to the outlier. In this thesis, two methods of displaying the information are developed. The first method (Display 1) shows the image from one standard deviation below the mean to about three above, with the images mean manipulated to be 25. This allows the viewer to see the speckle due to the grass and ground, and to see how the trees and targets are dispersed. The second method (Display 2) shows the image from the mean to 10 standard deviations above the mean. The image is manipulated so the mean is at 0, and 100 is 10 standards of deviation above the mean. This method tends to completely suppress speckle and weak signals from trees. This method is useful in showing how the

tree signatures are suppressed and the target signatures enhanced in each image by the WASAR Pre-Processing Algorithms. It should be noted that the processing done on the images in the display methods is not used in the target detection. The images are displayed with both data sets, using both display methods.

3.2.2 WASAR Pre-Processing Methods. In order to extract exploitable characteristics of WASAR data, such as a target's return varying with aspect angle, various algorithms are performed on the data before target detection. The algorithm is defined, and examples of the processed data displayed. As a point of reference, an image of unprocessed data is displayed in Figure 3.1. As discussed before, two display methods are used to show the images. Figures 3.1 (a) and (c) use Display 1. Figures 3.1 (b) and (d) use Display 2, the standard deviation method.

3.2.3 Mean Method (Mean). The first method attempted is simply to add each of the seven images together pixel by pixel, and divide each pixel in the resulting image by seven (the total number of images in the HH polarization). Thus, if X_n represents the n^{th} image, then

$$X_{mean}(i,j) = \frac{1}{N} \sum_{n=1}^{N} X_n(i,j), \tag{3.1}$$

and N is the total number on images in the data set. Figure 3.2 shows the resulting images from the mean method for Data Sets 1 and 2, with N=7.

3.2.4 Subtraction Method (Sub & Sub45). This method uses change detection. It has been theorized regardless of aspect angle, trees look approximately the same to a radar. Man-made objects, on the other hand, are known to change dramatically with azimuth

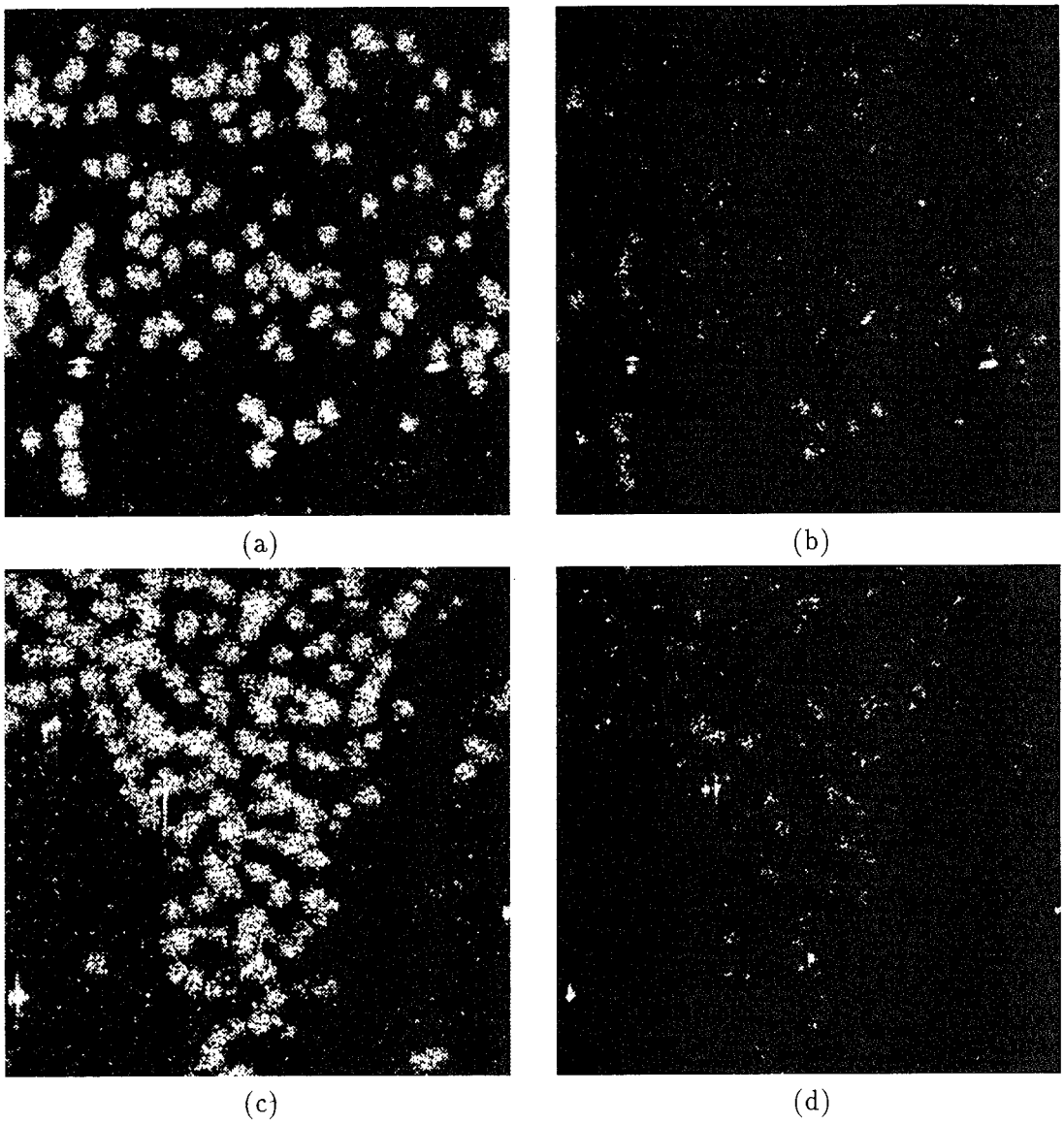

Figure 3.1 Unprocessed Data (a) Data Set 1, Display 1; (b) Data Set 1, Display 2; (c) Data Set 2, Display 1; and (d) Data Set 2, Display 2

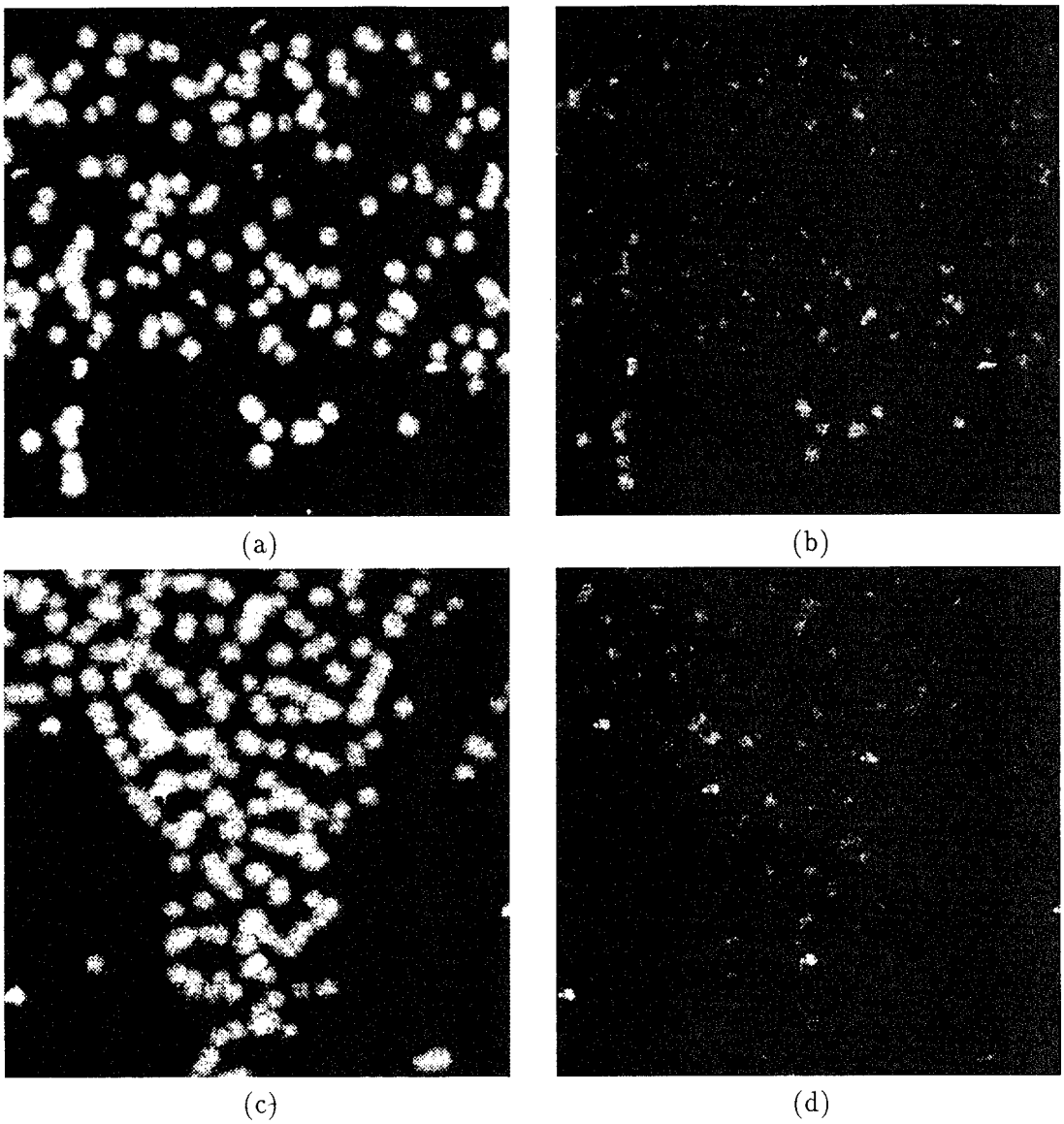

Figure 3.2 Data Processed by Mean Method (a) Data Set 1, Display 1; (b) Data Set 1, Display 2; (c) Data Set 2, Display 1; and (d) Data Set 2, Display 2

angle [10]. This is easily visualized when considering a cube-shaped metallic object. When such an object is illuminated along a flat face with SAR, a great deal of the incident energy is reflected back to the radar. Alternatively, when viewed from a corner between two faces, relatively less of the energy is returned. This simplistic explanation can easily be expanded to include angular objects such as trucks and tanks (see Figure 1.3). Thus, this method attempts to exploit the angular characteristic of man-made objects. One image is subtracted from another pixel-by-pixel, and the magnitude of the resulting image is used. If the targets are actually changing more than the trees from angle to angle, the magnitudes of the subtracted targets will on average be larger than that of the trees. All possible combinations of subtractions are used in order to exploit this characteristic, and the resulting images averaged. Again, with all seven images, where X_n is the n^{th} image,

$$X_{sub}(i,j) = \frac{1}{C} \sum_{n=1}^{N-1} \sum_{m=n+1}^{N} |X_n(i,j) - X_m(i,j)|, \tag{3.2}$$

where C is a constant with respect to N, and can be shown to be

$$C = \frac{N^2 - N}{2}.$$

In this case, N=7 and C=21. Figure 3.3 shows the data after processing with the Subtraction Method. A second method of subtraction attempts to further exploit the changes in man-made objects with angle, subtracting only those images 45° apart from one another. The reasoning behind this is that the maximum difference between a cube shaped reflector is at a 45-degree difference. Thus, with the available seven images, there are four possible

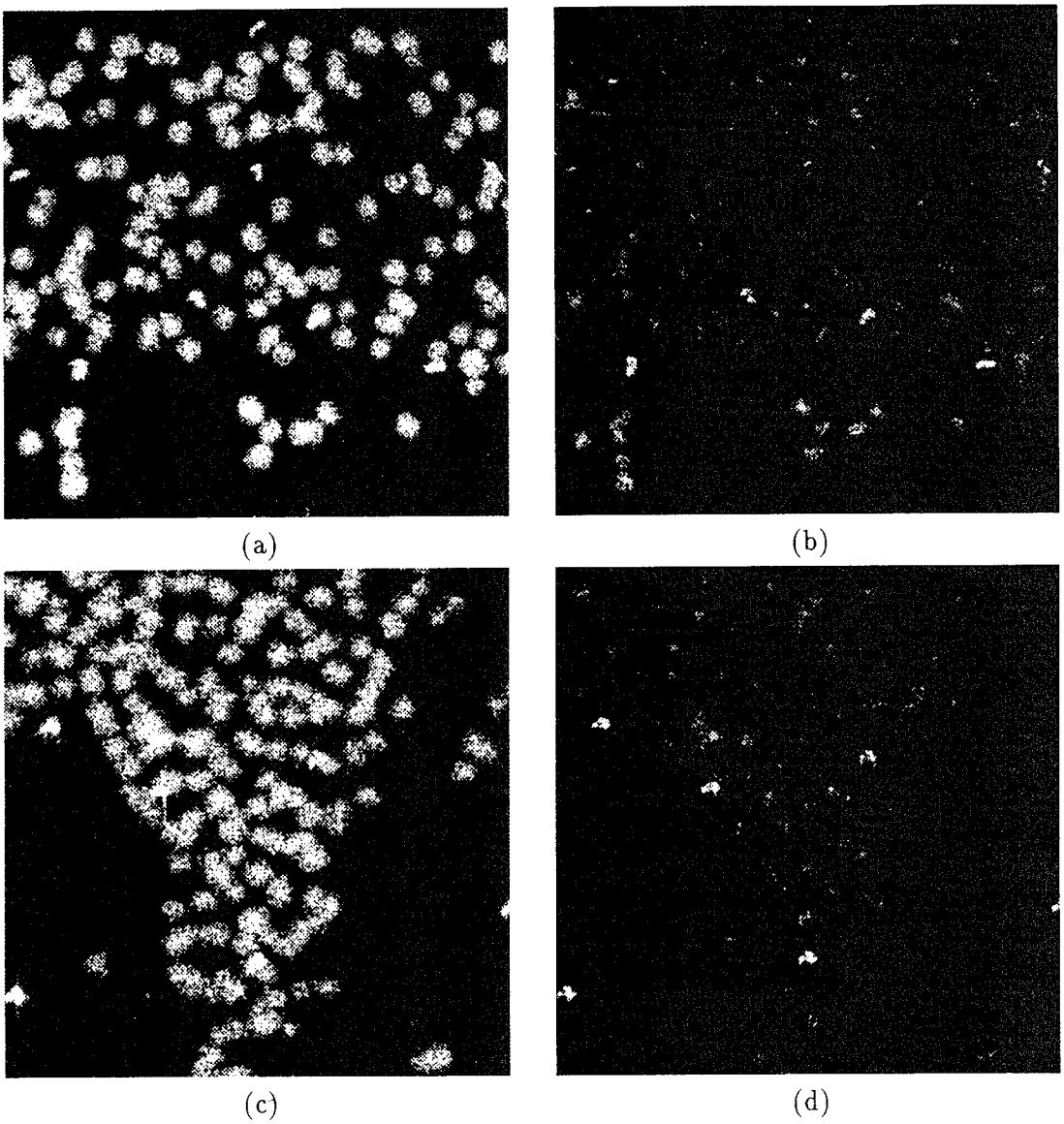

Figure 3.3 Data Processed by Subtraction Method (a) Data Set 1, Display 1; (b) Data Set 1, Display 2; (c) Data Set 2, Display 1; and (d) Data Set 2, Display 2

combinations of images 45° apart, and

$$X_{sub-45}(i,j) = \frac{1}{N}\sum_{n=1}^{N} |X_n(i,j) - Y_n(i,j)|, \tag{3.3}$$

where X_n and Y_n are 45° apart, and N=4. The 45° subtraction images can be seen in Figure 3.4.

3.2.5 Standard Deviation and Variance Methods (SDM & Var). The next two methods also exploit the angular characteristics of man-made objects. If the target to be detected is changing from angle to angle, and the trees are not changing as much, then the pixel-to-pixel standard deviation or variance of the targets should be greater than that of the rest of the image. Thus if the variance of the images is taken with respect to the mean image, then the average variance of the targets should stand out more than that of the surrounding clutter, and similarly for the standard deviation. The standard deviation, with X_n^* being the complex conjugate of X_n, is defined as

$$X_{std_dev}(i,j) = \frac{1}{N}\sum_{n=1}^{N} \sqrt{(X_n(i,j) - X_{mean}(i,j))^*(X_n(i,j) - X_{mean}(i,j))}. \tag{3.4}$$

The processed data is seen in Figure 3.5. The variance X_{var} is defined as

$$X_{var}(i,j) = \frac{1}{N}\sum_{n=1}^{N} (X_n(i,j) - X_{mean}(i,j))^*(X_n(i,j) - X_{mean}(i,j)), \tag{3.5}$$

with X_{mean} defined as before in Equation 3.1 and N=7. The variance method images are shown in Figure 3.6.

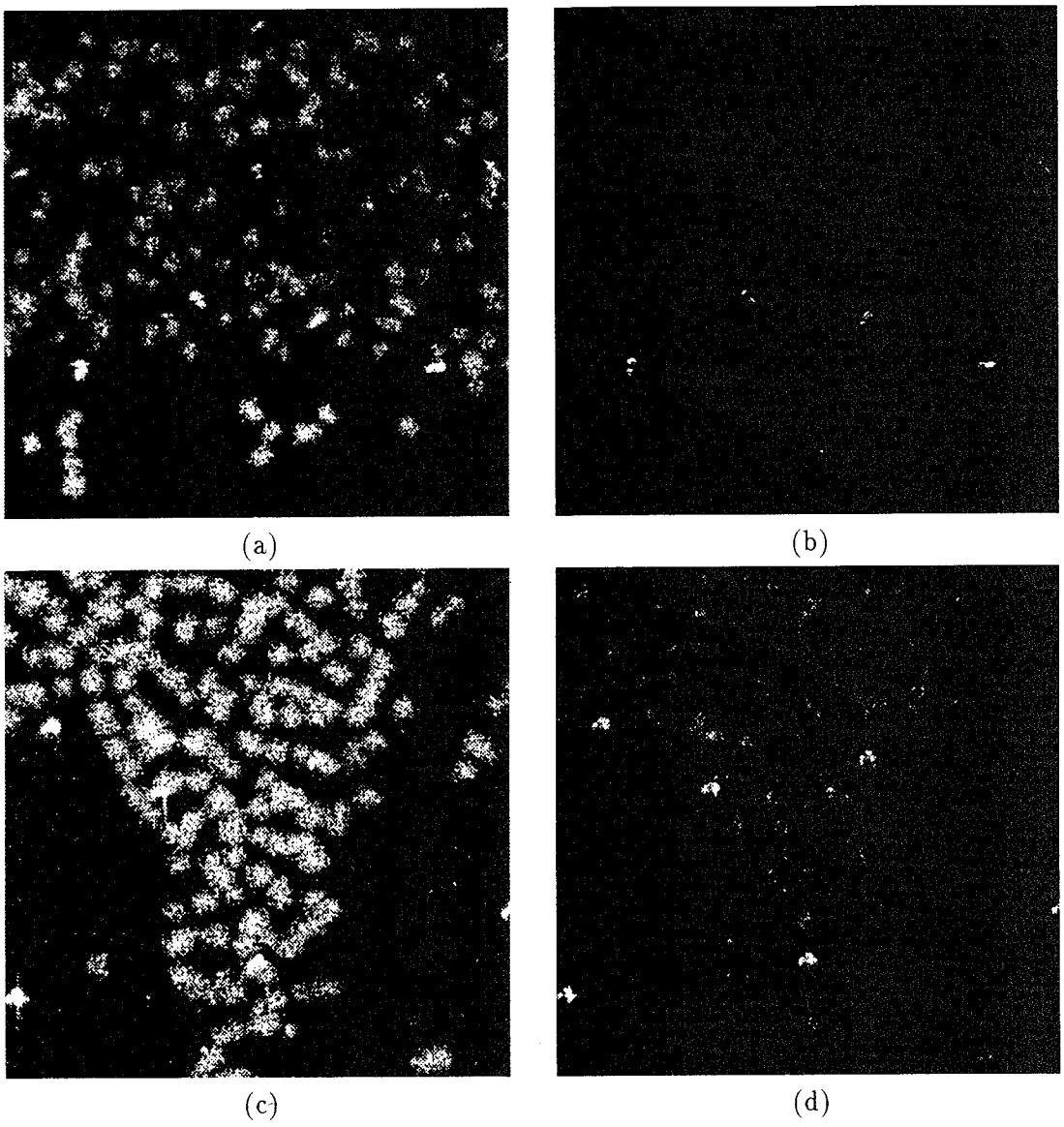

Figure 3.4 Data Processed by 45° Subtraction Method (a) Data Set 1, Display 1; (b) Data Set 1, Display 2; (c) Data Set 2, Display 1; and (d) Data Set 2, Display 2

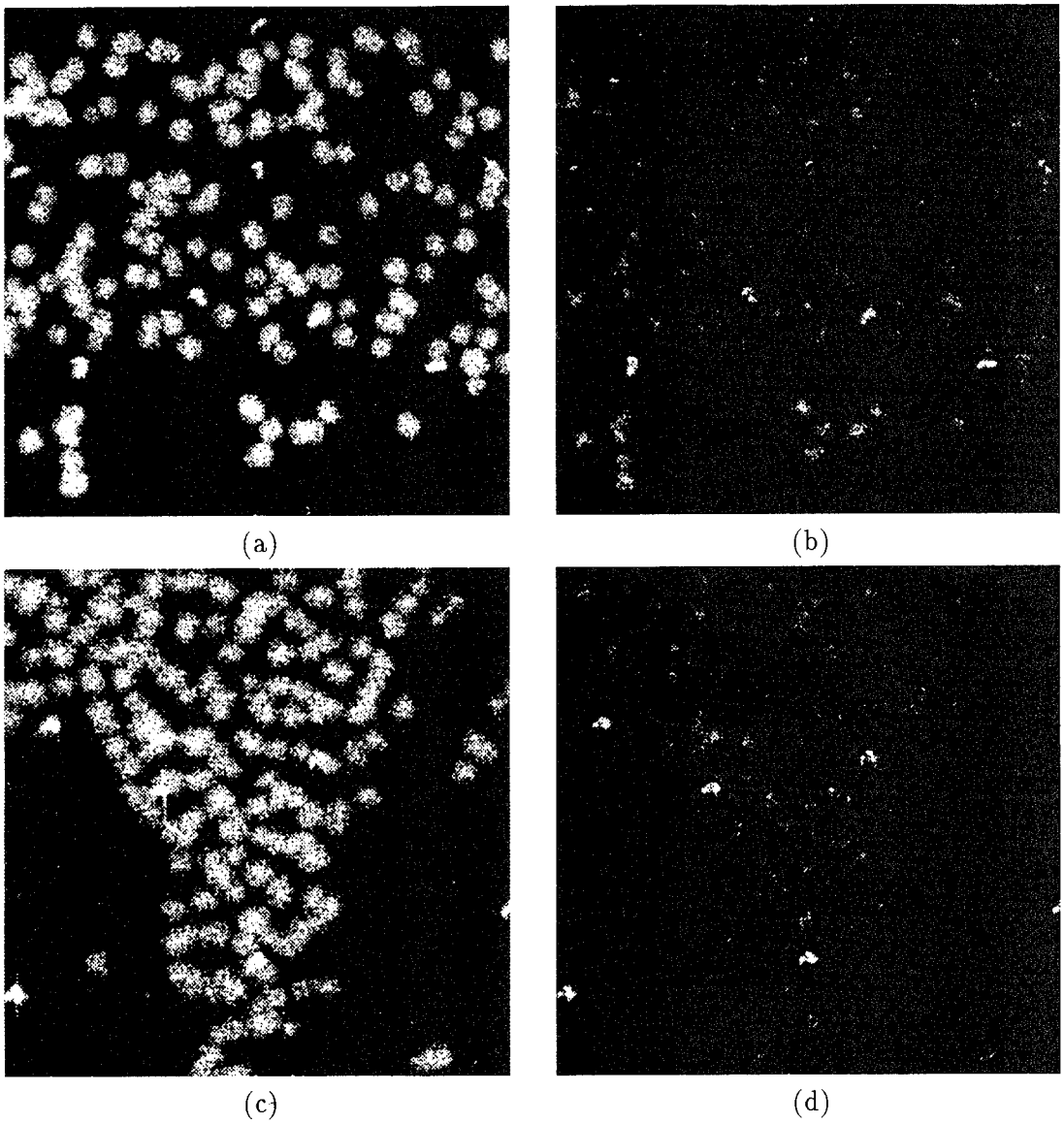

Figure 3.5 Data Processed by Standard Deviation Method (a) Data Set 1, Display 1; (b) Data Set 1, Display 2; (c) Data Set 2, Display 1; and (d) Data Set 2, Display 2

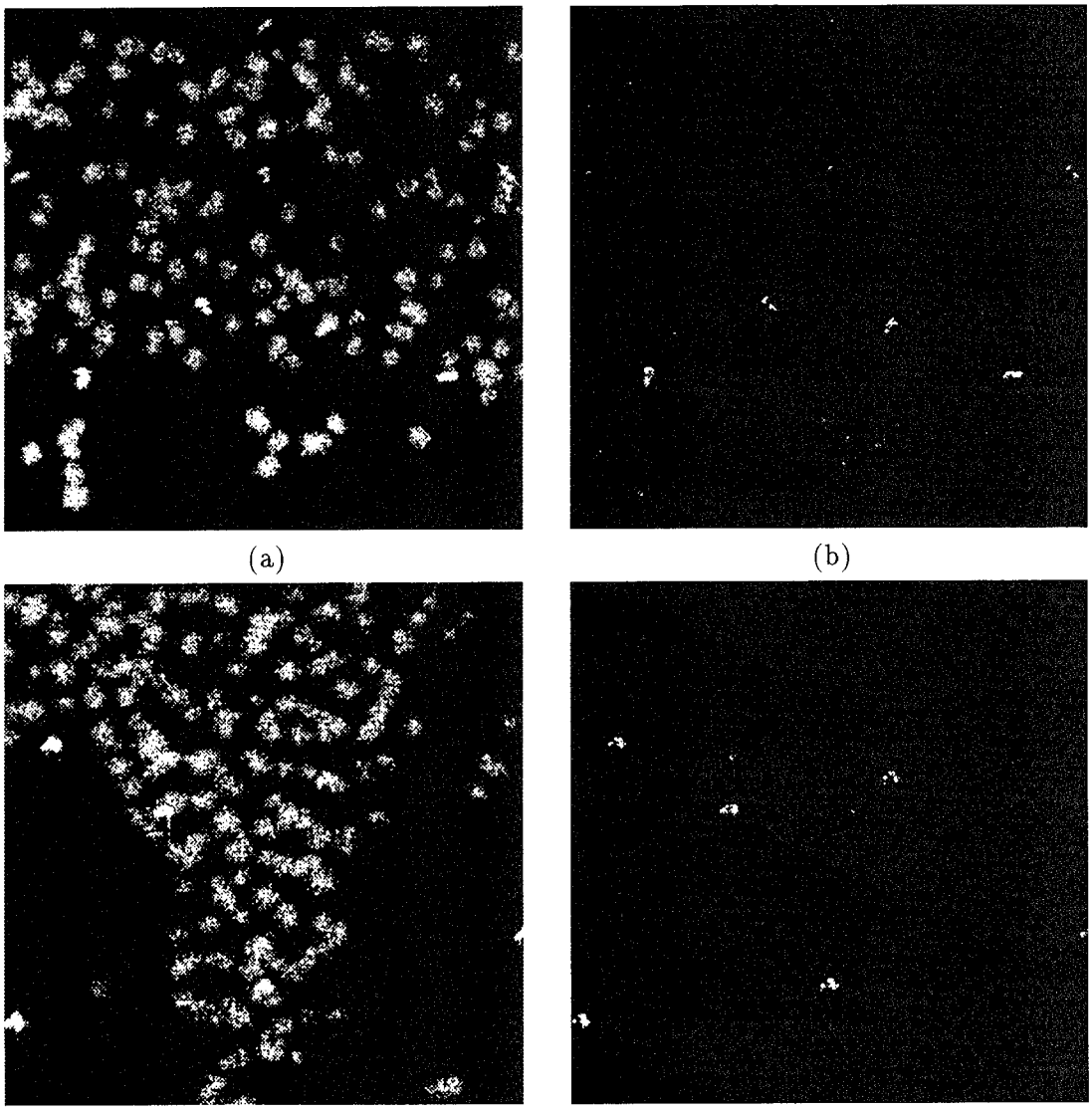

Figure 3.6 Data Processed by Variance Method (a) Data Set 1, Display 1; (b) Data Set 1, Display 2; (c) Data Set 2, Display 1; and (d) Data Set 2, Display 2

3.2.6 Subtraction of Powers Method (SPM). Another interesting processing method is similar to the subtraction of images method. The difference being the subtractions take place between the computed powers of each image, or

$$X_{pow_sub} = \frac{1}{C} \sum_{n=1}^{N-1} \sum_{m=n+1}^{N} |X_{n,pow}(i,j) - X_{m,pow}(i,j)|, \tag{3.6}$$

with $X_{n,pow}$ defined as

$$X_{n,pow}(i,j) = (X_n(i,j) - X_{mean}(i,j))^*(X_n(i,j) - X_{mean}(i,j)) \tag{3.7}$$

and C=21 since N=7. Figure 3.7 displays the data after processing by the SPM method.

3.2.7 Mean of Powers Minus Variance (MPMVM). The last method involves finding a mean variance, then computing each images power minus the mean variance, and finally averaging the magnitudes. This is expressed mathematically as

$$X_{mean_pow-mean}(i,j) = \frac{1}{N} \sum_{n=1}^{N} |X_{n,pow}(i,j) - X_{var}(i,j)|, \tag{3.8}$$

with $X_{n,pow}$ and X_{var} defined in equations 3.7 and 3.5, respectively. The images of the data processed by the MPMVM method are seen in Figure 3.8.

3.3 Statistical Analysis of Various Methods

A first measure of how the various detection methods perform is to compare their statistics with those of a single image. Novak [8, 9] states that a good measure for com-

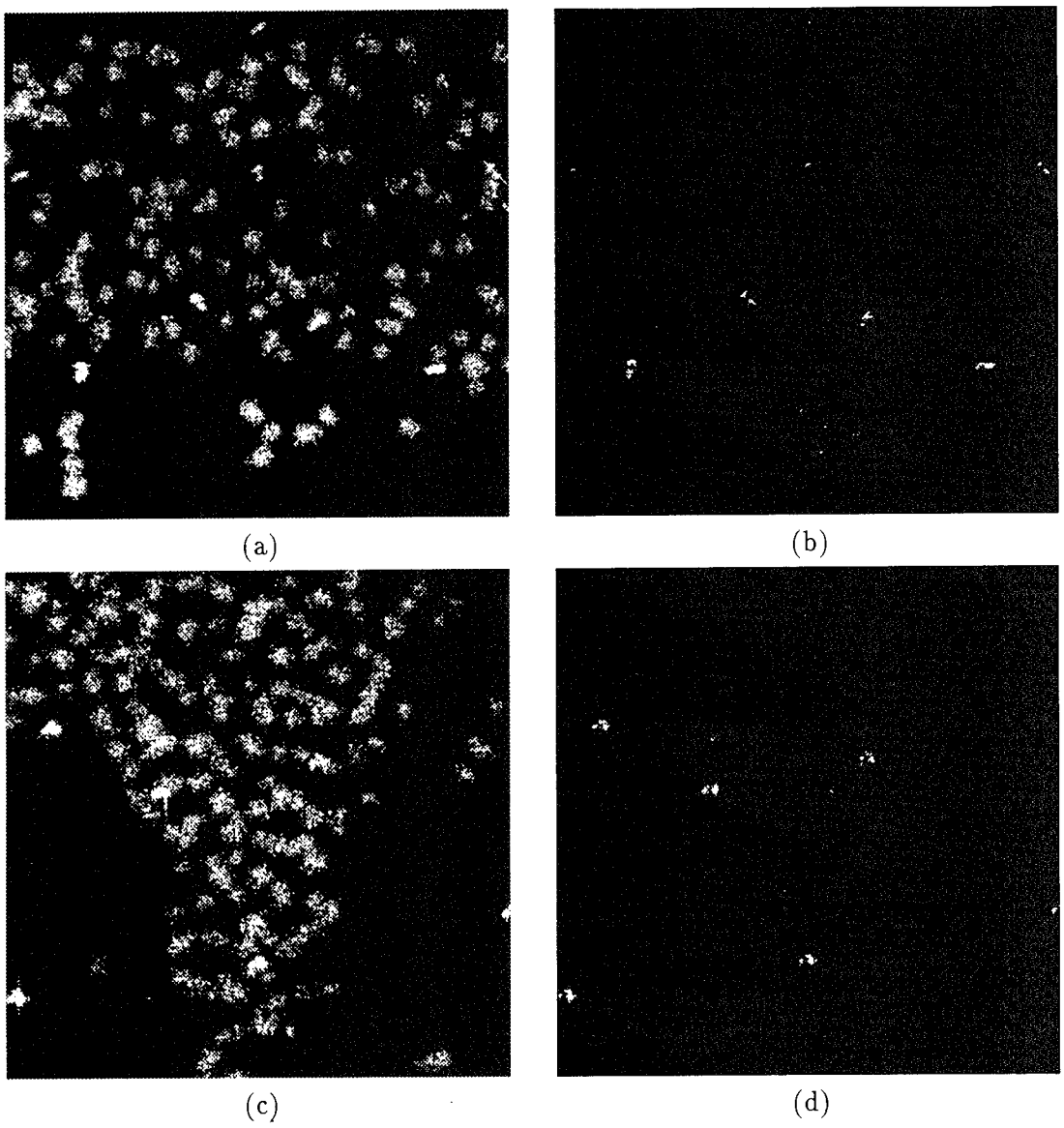

Figure 3.7 Data Processed by Subtraction of Powers Method (a) Data Set 1, Display 1; (b) Data Set 1, Display 2; (c) Data Set 2, Display 1; and (d) Data Set 2, Display 2

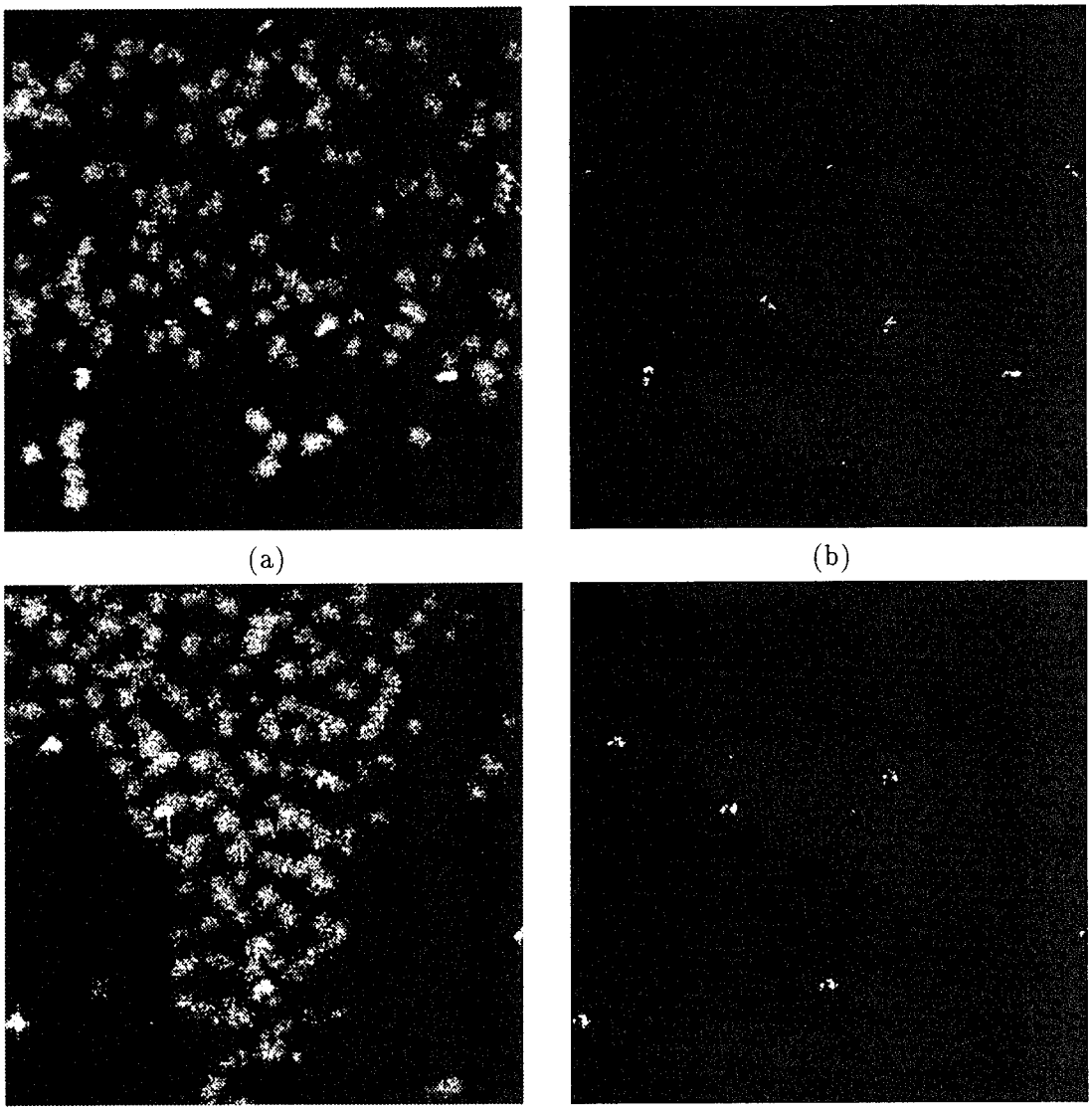

Figure 3.8 Data Processed by Mean of Powers Minus Variance Method (a) Data Set 1, Display 1; (b) Data Set 1, Display 2; (c) Data Set 2, Display 1; and (d) Data Set 2, Display 2

parison is the standard deviation to mean ratio (SMR);

$$SMR = \frac{\sigma}{\mu}, \tag{3.9}$$

with the image standard deviation defined as

$$\sigma = \frac{1}{MN-1}\sum_{i=1}^{N}\sum_{j=1}^{M}(X(i,j)-\mu)(X(i,j)-\mu)^*, \tag{3.10}$$

and the image mean defined as

$$\mu = \frac{1}{MN}\sum_{i=1}^{N}\sum_{j=1}^{M}X(i,j). \tag{3.11}$$

Notice that this statistic is for one image, i.e. the mean is the mean of all pixels in the respective image, not the WASAR mean defined in Equation 3.1. As the SMR goes down, the "detectability" of the target should increase. This is because as the SMR is reduced, the clutter does not have high frequency variations, therefore eliminating more false alarms. The standard deviation of the targets is found by taking a small portion of the image around each of the targets, finding the standard deviation of the smaller images, and finding the average target standard deviation. Ideally, the SMR is reduced by the various WASAR Pre-Processing methods. Other statistics shown are the targets variance and power, and the noise variance and power. The target variance is found in the same manner as the standard deviation, and the noise variance is found by removing the targets from the scene. Comparisons between the various processing methods are seen in Tables 3.1 and 3.2. The results in Table 3.1 indicate that little can be inferred from the change of target variance or power. However, it should be noted that the standard deviation to

Table 3.1 Statistics of Various Methods, Data Set 1

Method	Targ Var	Targ Pow	Noise Var	Noise Pow	SMR (dB)
SAR (0°)	88.0915	107.6635	1.7067	2.6565	3.8523
Mean	6.9203	15.5877	1.1186	2.0900	0.7523
Sub	10.3952	18.5418	0.4562	0.8746	1.0877
Sub45	29.2450	30.7240	5.1515	5.6738	2.3599
SDM	5.5611	9.5112	0.2048	0.3897	1.2811
VAR	3584.20	3891.0	2.3681	2.6853	1.8123
SPM	10523.0	11318.0	4.4150	4.9292	2.0124
MPMVM	7014.60	7500.4	2.2496	2.4998	2.1183

mean ratio (SMR) was reduced in all cases. This is one of the desired characteristics of processing mentioned earlier. Table 3.2 shows that little information about the algorithms

Table 3.2 Statistics of Various Methods, Data Set 2

Method	Targ Var	Targ Pow	Noise Var	Noise Pow	SMR (dB)
SAR (0°)	65.4793	97.7718	1.2833	2.2343	2.3975
Mean	8.4394	27.1155	0.8104	1.7755	0.4153
Sub	10.6645	24.8404	0.3460	0.7731	0.0206
Sub45	21.9188	40.7590	0.3920	0.8152	1.0865
SDM	5.5175	12.2150	0.1549	0.3435	0.1877
VAR	1843.30	2197.10	1.1000	1.4000	1.5500
SPM	4502.90	5188.10	2.1000	2.5000	1.7000
MPMVM	2825.90	3192.60	1.1000	1.3000	1.7900

can be gained from the variances and powers, while the SMR has been reduced. Being unable to judge performance by statistics alone, other methods are needed. The most enlightening method is to plot out the histograms of the targets and noise, which can be normalized to represent the approximate respective probability mass functions (PMFs). These results are discussed in Chapter IV.

3.4 Summary of Chapter

This chapter deals with various image processing methods for improving target detection characteristics. The methods are described in detail, and then used on the two data sets. Images from the processed data sets are displayed for comparing the methods. Various statistics are given and used to show the results of the processing. In Chapter IV the data resulting from the pre-processing techniques are used by target detection algorithms, which will give a definitive comparison between the processing methods.

IV. Target Detection

4.1 Overview

This chapter deals with target detection. First, basic detection theory is covered along with a discussion on probability of false alarms. The probability mass functions of the data resulting from the pre-processing methods are then displayed. These are used to show the improvements made by the processing algorithms towards more accurate target detection. Finally, the various methods are compared to one another by their actual detection performance.

4.2 Detection Theory

Before discussing detection of targets in the two data sets, it may be useful to discuss some of the basics of target detection theory as it applies to this thesis. Assume $x_1, x_2, \ldots, x_N$ denote N scalar measurements of the form $x_i = \theta s_i + n_i$, with s_i a known signal, n_i noise, and θ a parameter in the parameter space Θ. If $\Theta = \Theta_0 \bigcup \Theta_1 \bigcup \ldots \bigcup \Theta_{M-1}$ is a disjoint set covering the parameter space, then the hypothesis tests $H_i : \theta \in \Theta_i$ may be formed as

$$H_0 \textit{ versus } H_1 \textit{ versus } \ldots H_{M-1}.$$

This type of test is called a multiple, or M-ary hypothesis test. If $\Theta = \Theta_0 \bigcup \Theta_1$, then we would have a binary test. If the constant $\theta \in \Theta_0$, then we assume the system is in its zero state and hypothesis H_0 is in effect. Likewise, if $\theta \in \Theta_1$, hypothesis H_1 is in effect, or

$$H_0 : \theta \in \Theta_0 \textit{ versus } H_1 : \theta \in \Theta_1.$$

Also, if Θ_0 contains a single element θ_i, the hypothesis is said to be simple, otherwise it is composite. The detection problem is one of observing x_i, $i = 1, \ldots, N$, and deciding between $H_0, H_1, \ldots,$ or H_{M-1} [11].

In this case, our signal is the radar pulse. If a target is present in an illuminated "cell" (or pixel), then the returned pulse will be some multiple $\theta \in \Theta_1$ times the signal, plus added noise. Thus, when a target is present, θ is an element of Θ_1, and in the absence of a target θ is an element of Θ_0. Since the elements of Θ_1 can be a wide range of numbers depending on the type of target (or portion of a target) illuminated, and the elements of Θ_0 can vary depending on the reflectivity of the surroundings, this is a binary composite test of hypothesis.

4.2.1 Testing of Binary Hypothesis. If $\mathbf{X}$ is a random vector with distribution $F_\theta(\mathbf{x})$ and $\theta \in \Theta$ then a binary test of $H_0 : \theta \in \Theta_0 \text{versus} H_1 : \theta \in \Theta_1$ can be represented as

$$\phi(\mathbf{x}) = \begin{cases} 1 \sim H_1, & \mathbf{x} \in R \\ 0 \sim H_0, & \mathbf{x} \in A \end{cases} . \tag{4.1}$$

This means that if the measurement $\mathbf{x}$ lies in the rejection region R, the test function $\phi(\mathbf{x})$ is 1, and hypothesis H_1 is accepted. Otherwise, if $\mathbf{x}$ lies in the acceptance region A, then the test function equals zero and H_0 is accepted [11].

Now suppose $\theta \in \Theta_0$ but $\mathbf{x} \in R$, then H_0 would be rejected when in fact it was in force. This is called a type I error, or a false alarm. Figure 4.1 demonstrates the probability of false alarm (P_{fa}) between two Gaussian curves [11, 12, 5]. The shaded area represents the chance that $\mathbf{x}$ lies above the threshold, but H_0 is in effect, which is the definition of

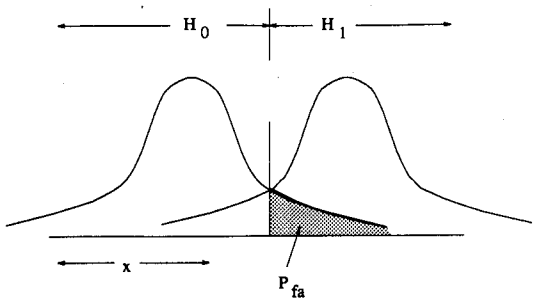

Figure 4.1 Example of Probability of False Alarm (P_{fa})

P_{fa}. It stands to reason that if the two curves were somehow separated from one another through some type of processing, then the P_{fa} would be lowered and detection performance would be improved. In this case the PMFs are not Gaussian, but the same principle holds; the farther apart the PMFs are, the lower the P_{fa} will be. Figure 4.2 (a) shows the actual histogram of the unprocessed SAR data. It is difficult to get any feel for the distribution of the data since the ratio of target pixels to noise pixels is very low, so the noise curve almost completely suppresses the target curve. Figure 4.2 (b) shows the histogram after it has been normalized to show the approximate PMF of the same data. The histogram is also truncated to show more detail. Figure 4.2 (b) gives a better understanding of how the data are distributed. It should be noted that the tails extend up to the value of 1. The x-axis corresponds to the thresholds used for target detection, which range from zero to one (0% to 100%). Figures 4.3 and 4.4 show the normalized histograms (and approximate PMFs) of the targets and noise in Data Set 1 and Data Set 2, respectively. The histogram of the original SAR data shows a large overlap in the PMFs, therefore having a larger P_{fa} for a set threshold. The various processing methods show varying amounts of improvements in the separation of the PMFs, therefore signifying probable improvements in detection characteristics. Notice that the histograms (and approximate PMF's) are actually lines

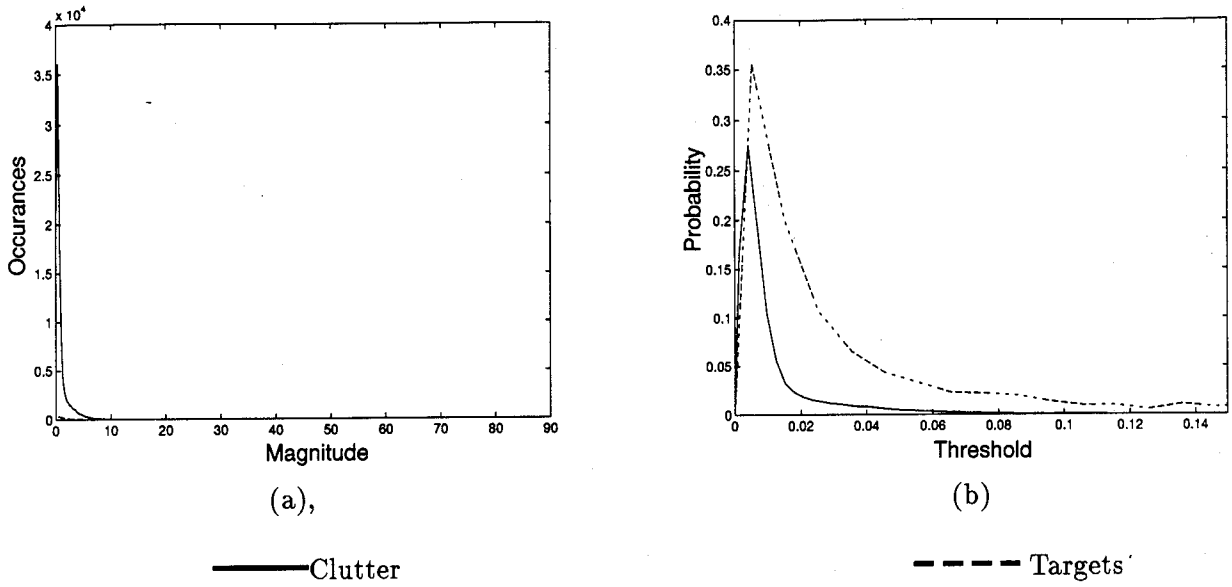

Figure 4.2 Correlation Between True Histogram and Normalized Histogram Meant to Approximate the Probability Mass Function of the same Data (a) Histogram of SAR (0^o) and (b) Normalized and Truncated Histogram of Same Data

connecting histograms. The apparent differences in areas under the functions are due to the fact that the histogram bin spacing is different for targets than for clutter.

Perhaps a more useful way of demonstrating the WASAR Pre-Processing methods effects on the target detection characteristics is to look at the receiver operating characteristics (ROC) of the data before and after processing. Figures 4.5 and 4.6 show the ROC curves for Data Sets 1 and 2, respectively. In Data Set 1 (Figure 4.5), it is seen that the unprocessed SAR data would actually perform worse than chance. All WASAR techniques, however, show better than chance ROC curves. Unfortunately, they do not reflect the detection characteristics seen later in this chapter. This is explained when the fact that this is a single data set is considered. These are only crude estimates of the ROC curves, so they only give rough estimates of what the actual ROC curves would be. Also,

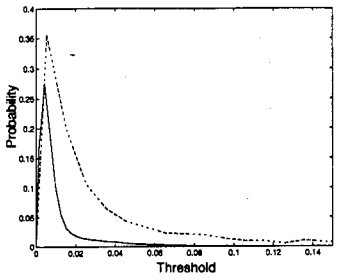

SAR (0°), HH

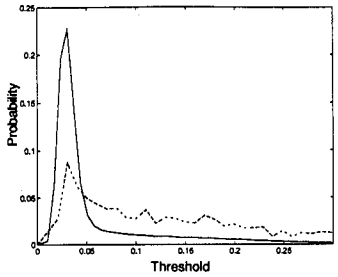

Mean

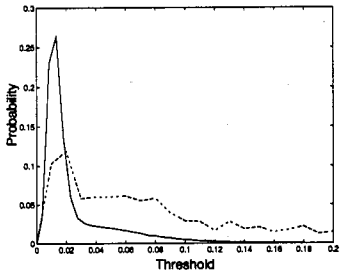

Sub

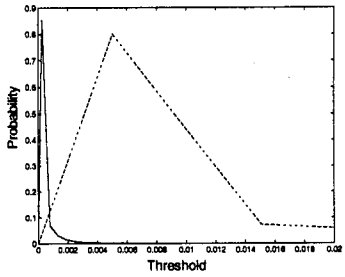

Sub45

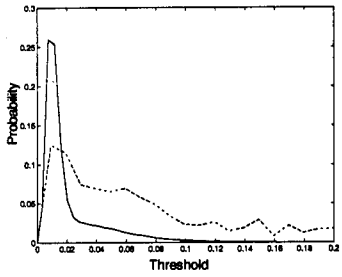

SDM

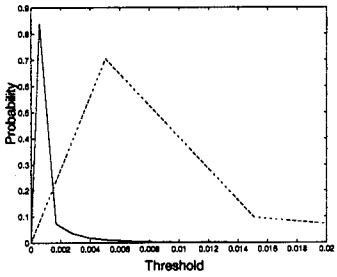

VAR

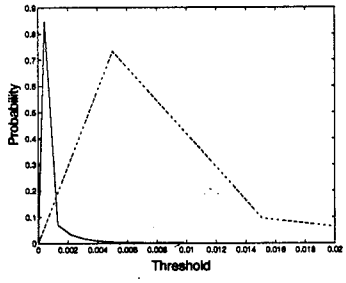

SPM

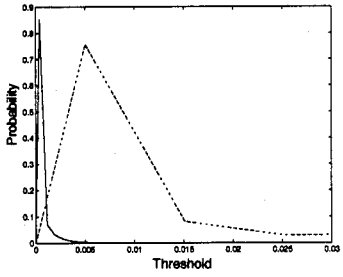

MPMVM

——Clutter Probability Mass Function

- - - - Target Probability Mass Function

Figure 4.3 Histograms (Approximate PMFs) of Processed Data, Data Set 1 (Difference in area under PMFs is due to differing histogram bin spacing)

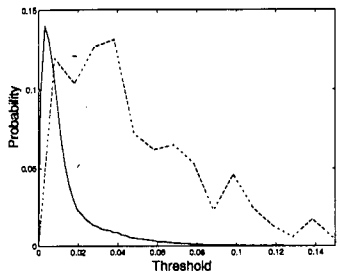

SAR (0°), HH

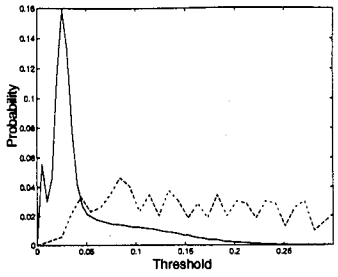

Mean

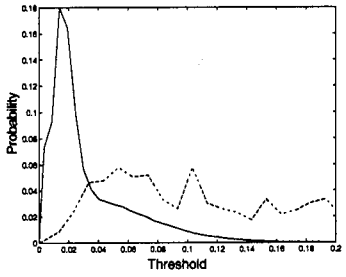

Sub

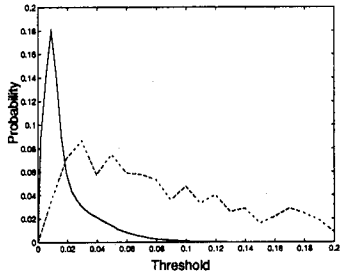

Sub45

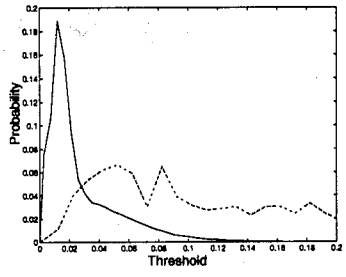

SDM

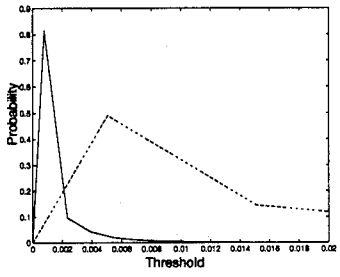

VAR

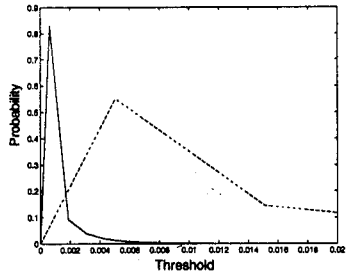

SPM

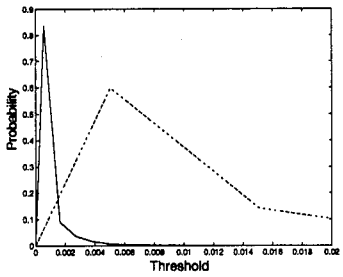

MPMVM

——— Clutter Probability Mass Function - - - - Target Probability Mass Function

Figure 4.4 Histograms (Approximate PMFs) of Processed Data, Data Set 2 (Difference in area under PMFs is due to differing histogram bin spacing)

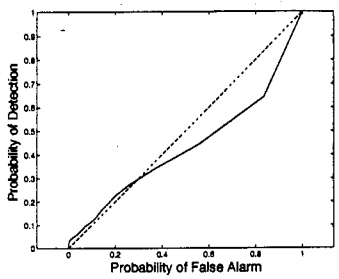

SAR (0°), HH

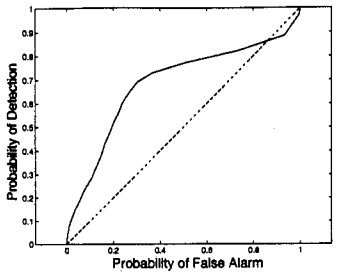

Mean

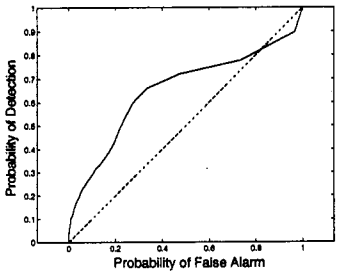

Sub

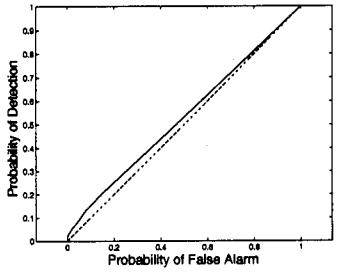

Sub45

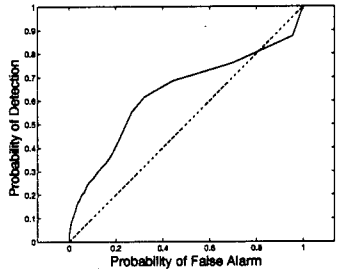

SDM

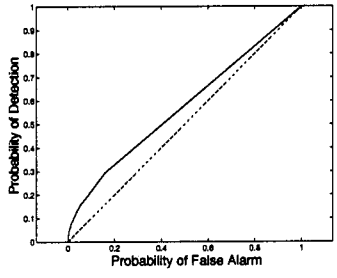

VAR

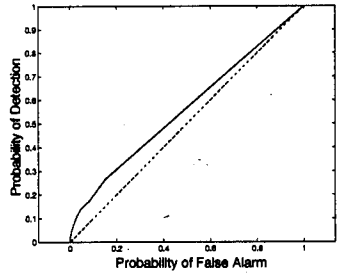

SPM

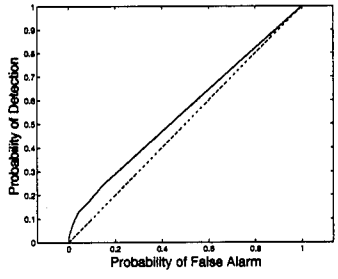

MPMVM

——(ROC) - - - - Chance Line

Figure 4.5 Receiver Operating Characteristics, Data Set 1

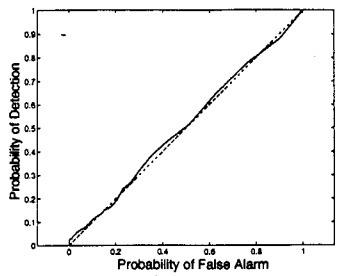

SAR (0^o), HH

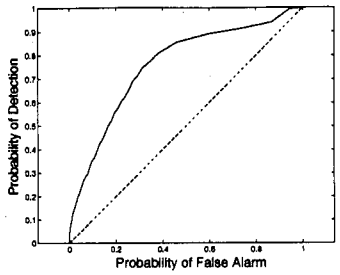

Mean

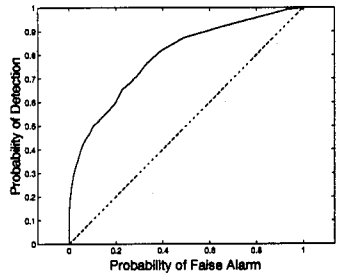

Sub

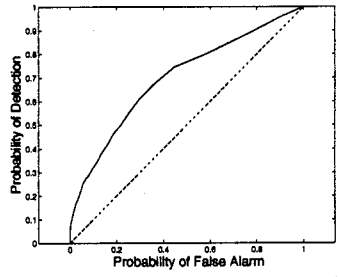

Sub45

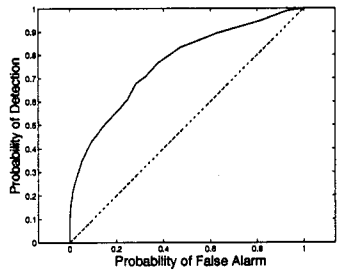

SDM

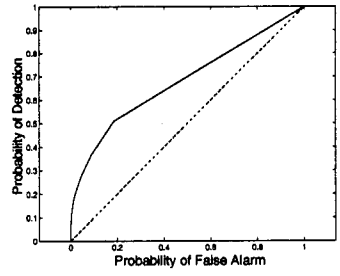

VAR

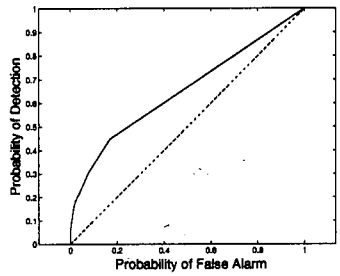

SPM

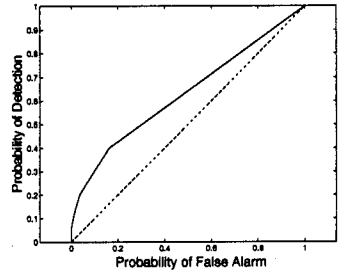

MPMVM

——(ROC) - - - - Chance Line

Figure 4.6 Receiver Operating Characteristics, Data Set 2

the ROC curves do not reflect the fact that in some instances, such as the Subtraction of Powers Method (SPM), all targets are detectable past the point of the threshold where no false alarm occur. Figure 4.6 reflects similar results. The SAR data gives a ROC even with chance, while all WASAR methods show marked improvement.

4.3 Threshold Detection

The method of detection in this thesis is threshold detection. Threshold detection simply sets a number as the threshold, and considers pixels with a magnitude greater than that number to contain a target. Pixels with a magnitude lower than the threshold are considered clutter. Grouping of the coordinates of detected pixels is then performed to eliminate redundant hits on targets and trees. For target grouping, the average radius of the targets is approximated using known target locations and estimating size from the images. Any hits within that grouping are considered as a detected target, and all counted as one target. For false alarms, the grouping is adjusted until the false alarms occur approximately once per tree detected, so the same tree is not counted twice. This turns out to be valid since the false alarm grouping is smaller than the target grouping. Target grouping is necessary since two tanks cannot be centered one or two feet from each other. So if the false alarm grouping is made to be as large as the targets, fewer false alarms will occur. It should be noted that simply saying a threshold is applied to an image is misleading, since it is not measuring radar return magnitude in all methods. For instance, in the variance method (VAR), the detection algorithm considers every pixel with a variance above the threshold as a target. So the algorithm in this case is checking variance, not magnitude.

There are two ways to set the threshold. The first (detect2.m in Appendix A) sets the threshold as a percentage of the range of the image. The threshold can range from 0 to 1 (or 0% to 100%). Basically, it takes the maximum value pixel minus the minimum value as the range of the picture, and the threshold is a percentage of that range. So assuming an image with a threshold of 0.5 (50%), and pixels ranging from 1 to 100, the algorithm considers every pixel greater than 50 as a target. If the threshold is set at 0 every pixel is detected, and at a threshold of 100 one pixel is detected. This turns out to be an advantage when comparing the various processing methods. The drawback, as with any distribution, is that a large outlier could distort the results, causing one pixel to cover the upper third of the threshold.

The second method (detect3.m in Appendix A) simply considers a number of standards of deviation above (or below) the mean of the image. The threshold in this case can theoretically range from $-\infty$ to ∞. So with a threshold of 3, the algorithm considers every pixel with a value greater than three times the standard deviation plus the mean as a target. The advantage of this method is that outliers do not have such a large effect on the threshold ranges as in the previous method. The drawback is that it would be harder to pick the number for the threshold such that you get all of the pixels detected (or rejected).

4.4 Detection Performance of WASAR Pre-Processing Methods

In order to quantify the performance of the various processing methods, each WASAR Pre-Processing method is given the data set and a range of values for the threshold. The methods then return a vector containing the possible targets for each threshold. This possible target vector is then manipulated as mentioned earlier to eliminate repeated de-

tections and false alarms. Since the percentage thresholding method lends itself to easily covering all pixel ranges, it is used. The performance of the various methods can be seen in Figures 4.7 and 4.8. The solid horizontal lines at 8 and 6 on the vertical axes are there to show the number of known targets in the first and second data sets, respectively.

It should be noted that in Figure 4.7 (Data Set 1) the algorithms are necessarily halted after 20 false alarms, regardless of weather all targets are detected. In Figure 4.8 (Data Set 2) the algorithms are halted after only 10 false alarms since by then all methods detect all targets. Also note that the false alarm curves shift around. Some shifting is expected from the processing, but not this amount. This is an example of how the outliers change the threshold axis significance. If the number of standard deviations method is used to set the threshold, the false alarm curves would be expected to be closer to the same areas. But then the question of what range to give the threshold axis arises. To get similar looking plots using the second thresholding method, the ranges of the threshold axis would have to be varied greatly. The performance figures verify that the WASAR Pre-Processed data gives better detection characteristics, as predicted earlier by the PMFs. Table 4.1 shows some important numbers that can be seen in the graphs of Figure 4.8. A similar table is not presented for Data Set 1 for reasons to be explained. The first column is the threshold (threshold ranges from 0 to 1) at which all known targets are detected. The second column gives the threshold at which the first false alarm is detected. The third column is the difference of the first two, and the fourth is the threshold at which more than 10 false alarms are detected. The final column gives the difference between the threshold at which all targets and more that 10 false alarms are detected. The third and fifth columns

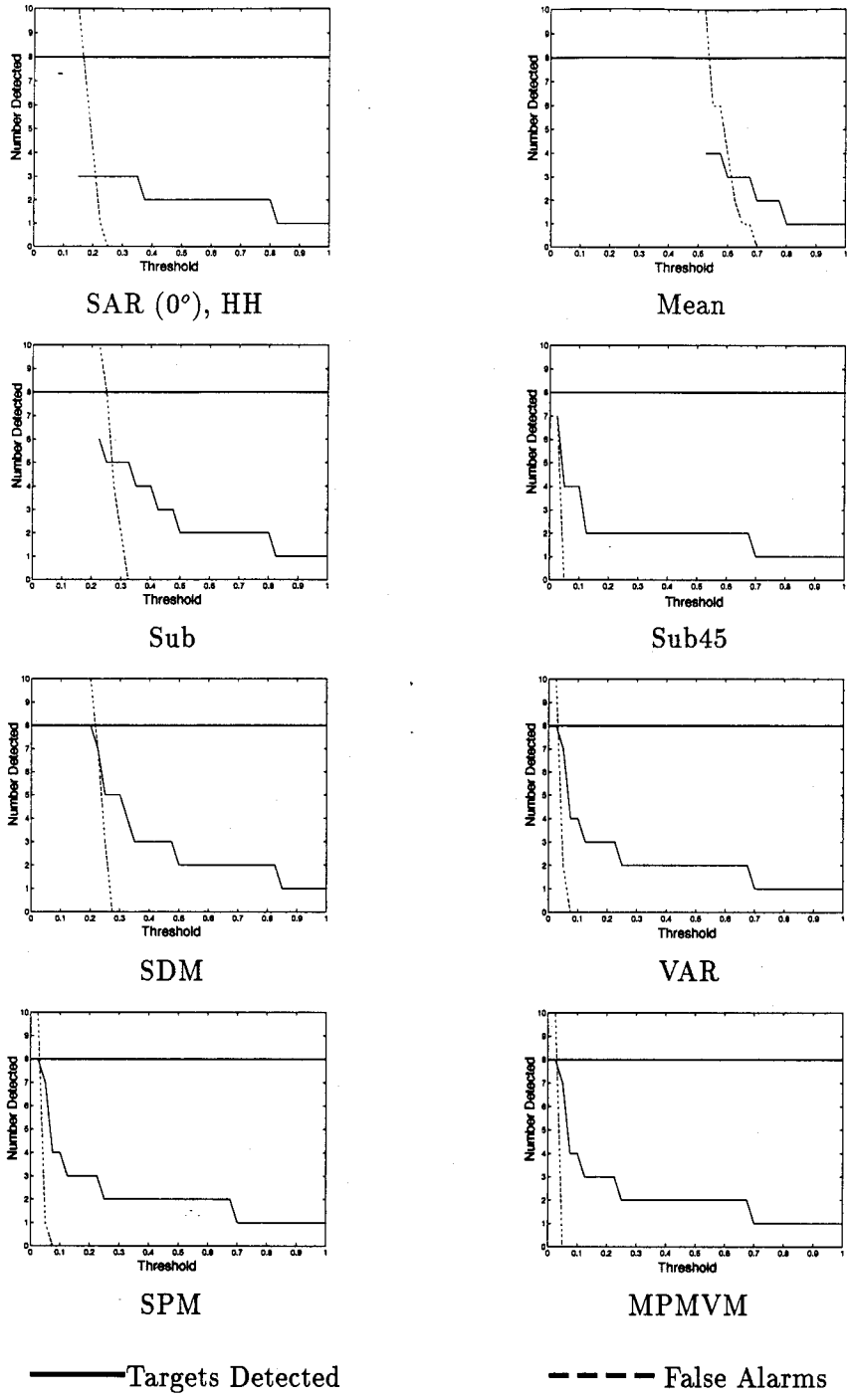

Figure 4.7 Performance of Various WASAR Detection Methods, Data Set 1. The line at 8 Detections on the vertical indicate there are 8 known targets. The threshold is set as described earlier as a percentage of the maximum pixel value.

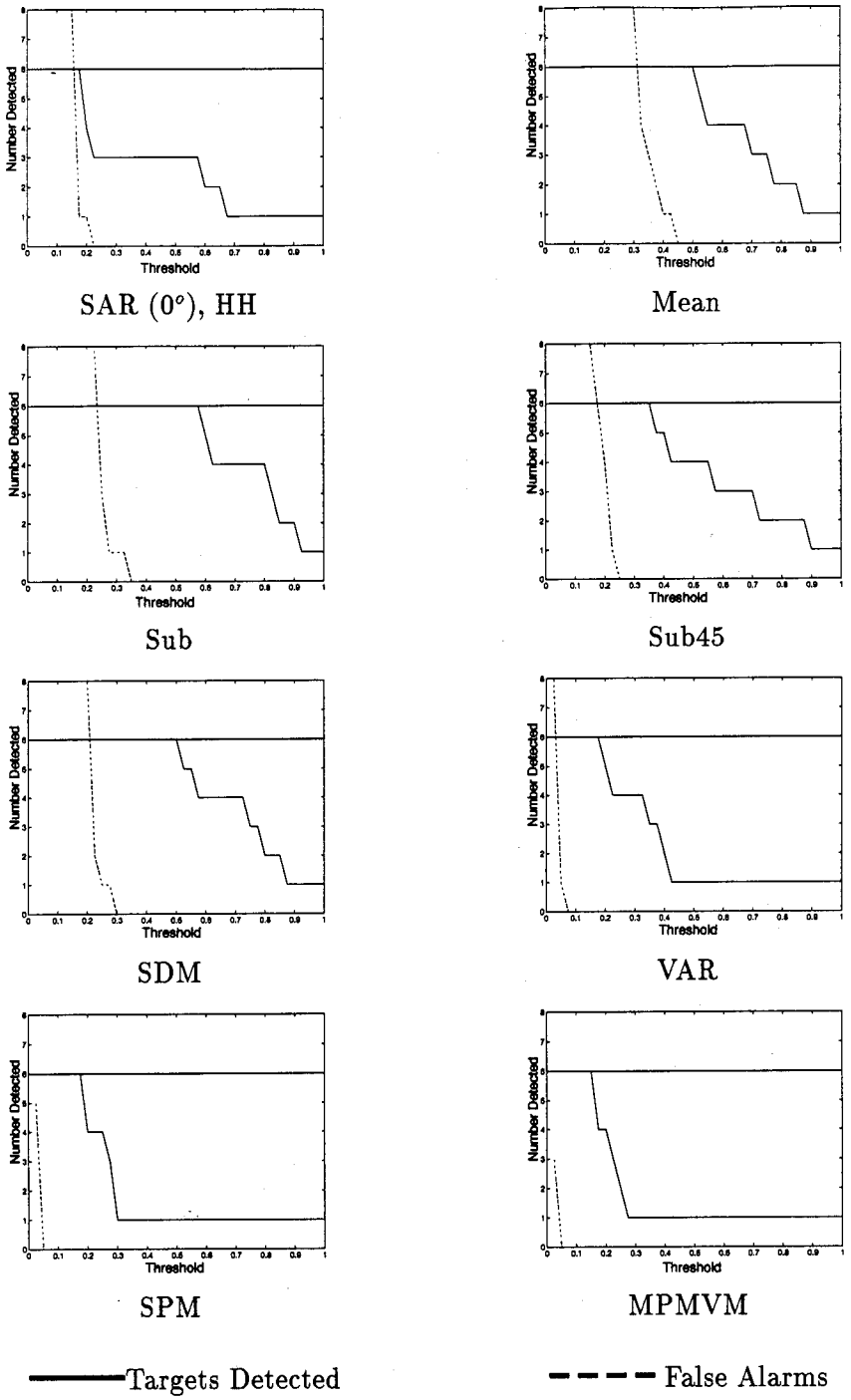

Figure 4.8 Performance of Various WASAR Detection Methods, Data Set 2. The line at 6 Detections on the vertical indicate there are 6 known targets. The threshold is set as described earlier as a percentage of the maximum pixel value.

Table 4.1 Performance of Various Methods, Data Set 2 (N/A signifies data not available)

Method	Threshold at which all Targets are Detected	Threshold first False Alarm Detected	Difference between all Targets Det and first FA	Threshold at which 10 FA Detected	Difference between all Targets det and 10 FA
SAR (0°)	0.1750	0.2000	-0.0250	0.1250	0.0500
Mean	0.5000	0.4250	0.0750	0.3000	0.2000
Sub	0.5750	0.3250	0.2500	0.2250	0.3500
Sub45	0.3500	0.2250	0.1250	0.1500	0.2000
SDM	0.5000	0.2750	0.2250	0.1750	0.3250
VAR	0.1750	0.0500	0.1250	0.0250	0.1500
SPM	0.1750	0.0250	0.1500	N/A	N/A
MPMVM	0.1500	0.0250	0.1250	N/A	N/A

are of importance because they give a metric for comparison between the various methods. Data Set 1 gives many more false alarms than Data Set 2, so most methods are unable to detect all targets before the algorithm ended due to false alarm saturation (in this case 20 false alarms). This is the reason a similar table is not constructed for Data Set 1, since it would be filled with "N/A"s. The difference between all targets detected and the first false alarm detected would seem to be a good metric. By this metric, Table 4.1 seems to indicate that the Subtraction (Sub) method and the Standard Deviation method (SDM) did the best job of extracting target signatures.

Figure 4.9 shows the correlation between the histograms in Figures 4.3 and 4.4 and the performance graphs in Figures 4.7 and 4.8. These particular histograms and performance curves are for the 0°, SAR data from Data Set 1. Figure 4.9 (a) is the performance curve for the unprocessed method SAR. Figure 4.9 (b) is its corresponding histogram of both noise and targets, while (c) is the targets data histogram and (d) is the noise histogram. Note that Figure 4.9 (a) shows a target at 1 and a false alarm at 0.25. These

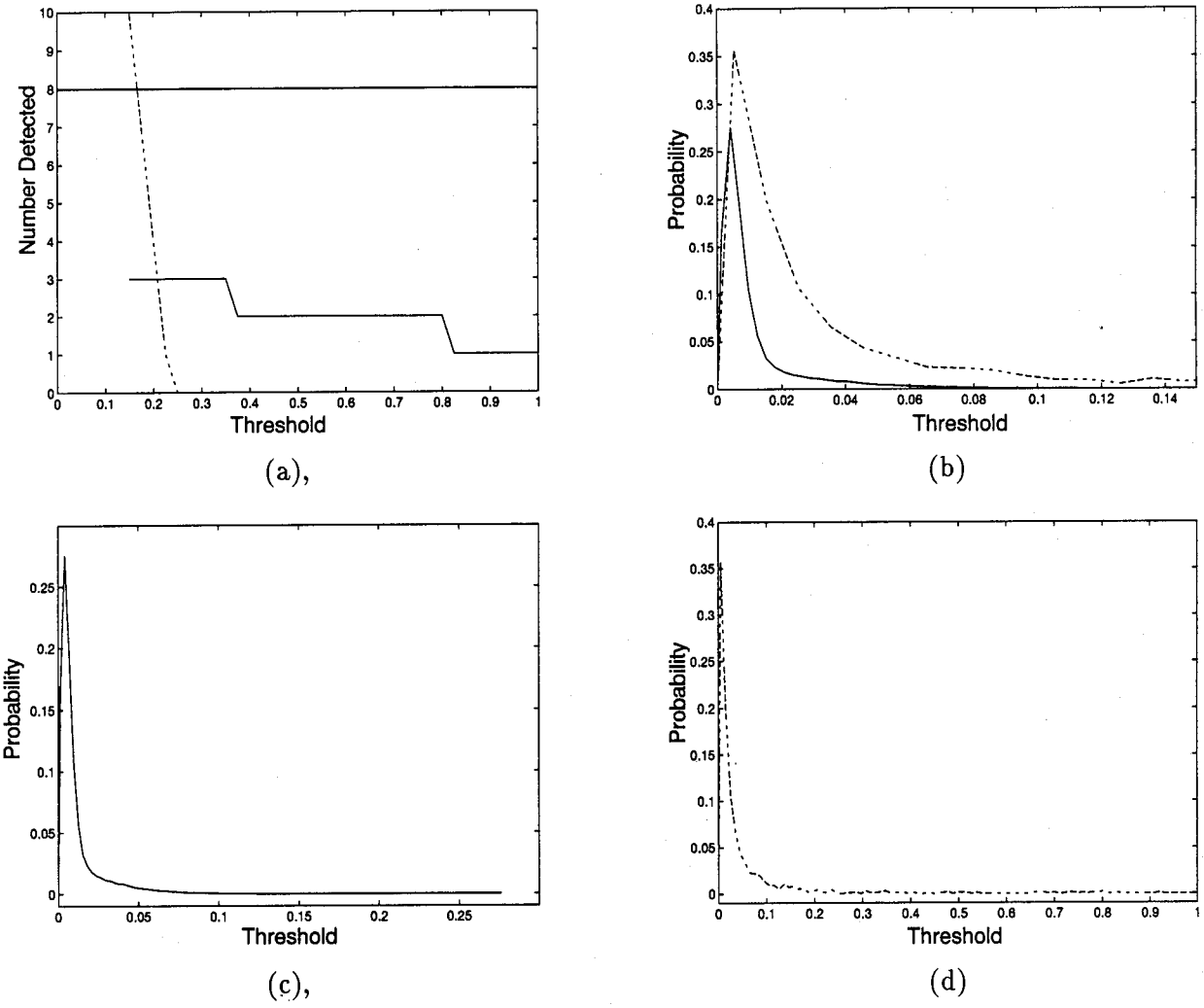

Figure 4.9 Correlation Between Histograms and Performance Graphs of the Unprocessed Data (Data Set 1, 0°, HH, SAR (a) Performance of SAR, (b) Histogram of SAR (0°), (c) Histogram of Clutter Data, and (d) Histogram of Target Data

correspond to the values of the histograms in (c) and (d). Part (c) shows that the noise histogram's tail goes out just past the normalized value 0.25, accounting for the first false alarm. After that, the other points shown on the noise histogram as you go down the x-axis toward zero account for more and more false alarms. Similarly, the target histogram in (d) shows a data point at normalized value 1, which is also where the first detection occurs.

4.5 Summary of Chapter

In this chapter basic detection theory is covered, and some insight on probability of false alarms is discussed. The probability mass function is then described and histograms displayed to show the improvements made towards more accurate target detection. Finally, the various methods are compared to one another by their actual detection performance graphically and numerically.

V. *Findings and Conclusions*

The final chapter of this thesis is dedicated to presenting results of this research. Conclusions on the performance and viability of WASAR are discussed, and several recommendations for improvements and future work are made.

5.1 Results of Research

The purpose of this thesis was to improve detection characteristics by exploiting the inherent changes in the scattering from targets with respect to aspect angle. Several methods were developed to accomplish this. With the assumptions that Wide-Angle SAR data was available, techniques to rotate the data to the same aspect-angle were developed. With the data properly registered, various pre-processing algorithms were employed to improve the probability of detection of targets while reducing the probability of false alarm. The processed data was then used in threshold detection to quantify the improvements made by each.

The difficulty in presenting results from this research was that there were few metrics (or measurements) that show the improvements. The best determination of the improvements was how the processed data performed in the target detection process. These results were presented in Figures 4.7 and 4.8. In Figure 4.7 (Data Set 1), the unprocessed Original SAR data was shown to have very poor performance characteristics, detecting less than half of the known targets at the false alarm saturation point (more than 10 false alarms). All WASAR methods were shown to improve upon this performance, with several of them detecting all targets before false alarm saturation. The improvements in detection charac-

teristics was even more visible in Figure 4.8. The unprocessed original SAR data reached 100% target detection at the same time false alarms were beginning to be detected. However, all WASAR methods detected all targets before detecting any false alarms, some detecting all targets up to 20% of the threshold above the first alarm. Specifically, the Subtraction method and the Standard Deviation method performed much better than the standard SAR method.

The detection of obscured ground targets was clearly made easier through the use of WASAR methods. The purpose of this thesis was to study how WASAR could be used to improve detection capabilities. The results of Chapter IV clearly indicated that improvements were made, and demonstrated the promising potential of WASAR.

5.2 Recommendations

While this thesis showed that marked improvement over SAR could be made with WASAR, it was only a basic study and much remains to be done. This research concentrated only on the processing of the different angle images of a scene. Novak showed that speckle-reduction methods using fully-polarimetric images give large reductions (up to 3dB) in standard deviation to mean ratios, while improving detection capabilities [6, 8]. Work should be performed on combining methods of speckle reduction and WASAR Pre-Processing. More information could be utilized through the use of a fully polarimetric WASAR detection scheme, as opposed to a WASAR scheme or a fully-polarimetric scheme alone. Results of this thesis also need to be verified by repeated testing with various data sets.

Statistics of the processed data must be studied and modeled. Attempts to show how the processing improves the data through statistics failed, due to an inaccurate model for the statistics. If the statistics of the data can be modeled accurately, better metrics could be devised to measure improvements. To do this, many realizations of the same scene and of different scenes must be produced. Repetitive data sets would help to verify the distributions of the target and clutter data.

Only the basic principles of target detection necessary for simple threshold detection is covered in this thesis. More advanced principles, such as finding a minimum variance unbiased estimate of the target parameter θ, could provide even better performance. This problem fits the criteria for a uniformly most powerful test [11], which could also lead to better results.

It may be possible to eliminate the 90^o swath of data used in this thesis. Performance of the Subtraction method (Sub) was better than that of 45^o Subtraction (Sub45). This was an unexpected result. As explained earlier, the greatest change between angles was expected at 45^o. But since this proved to not be the case, perhaps images taken with only a few degrees azimuth angle separation would perform equally as well.

Grouping of pixels should improve upon the advancements made here. By adding up neighboring groups of pixels (or averaging), the tree signatures should be reduced further. It stands to reason that some of the target signature will be lost, but most targets are many pixels in area, and averaging would only weaken the outer pixels.

5.3 Conclusions

WASAR is an interesting and promising field. This thesis shows that improvements over common SAR are made even with the most simple WASAR methods. More testing of WASAR methods on various data sets and the creation of more optimal WASAR Pre-Processing methods may prove WASAR to perform even better. Combinations of WASAR and fully-polarized SAR would certainly give even better results. With the improvements made in target detection characteristics through the use of WASAR Pre-Processing methods, WASAR is a valid and viable concept.

Appendix A. Computer Routines

The following computer routines are referenced in the thesis. They are matlab.m files, and a short description of their function is included at the top of each file.

A.1 Rotation of Images

A.1.1 Nearest Neighbor Method.

```
%%     FUNCTION rotation.m
%  Purpose:  Rotates an image input by "number" of fifteen degree increments.
%            Also cuts image down to overlapping square region.
%  Called by: rot.m
%  Quirks:
%    1) Uses short cut for 0 and +/- 90 degree rotations.


function [temp2] = rotation(temp1,number)

% number indicates the number of 15 degree increment rotations.
  phi = number * (-pi/12);   % angle of rotation

% (a,b) central point of rotation
  a = round(size(temp1,1)/2);
  b = round(size(temp1,2)/2);

if phi == 0
  temp2 = temp1;  % 0 degree short cut
elseif phi == pi/2
  temp2 = rot90(temp1,-1);  % 90 degree short cut
elseif phi == -pi/2
  temp2 = rot90(temp1,1);  % 90 degree short cut
else
  temp2 = min(min(temp1)) * ones(size(temp1,1),size(temp1,2));
  for i=1:size(temp2,1)
    for j=1:size(temp2,2)
      r = sqrt((i-a)^2 + (j-b)^2);
      theta = atan2((j-b),(i-a));
      x = round(r * cos(theta + phi)) + a;
      y = round(r * sin(theta + phi)) + b;
      if x>=1 & x<=size(temp1,1) & y>=1 & y<=size(temp1,2)
        temp2(i,j) = temp1(x,y);
```

```
      end
    end
  end
end

% cutting down image to square image of overlapping region
  l = ceil(a - round(sqrt( (a^2) / 2 )));
  u = floor(size(temp1,1) - l);
  temp2 = temp2(l:u,l:u);
```

A.1.2 Interpolation Method.

```
%% FUNCTION roti2.m
%  Purpose:  Rotates an image by angle passed as a parameter.  Also
%  cuts image down to size.  In order to get a close approximation to the
%  actual value, interpolates image first.
%  Calls: MATLABS interpolation program.
%  Specs: Interpolation performed by parameters L, E, and alpha.
%         Raising L and E greatly increase computation time.


function[dataout]=roti2(data,azang,L,E,alpha)

%% Error control
if azang<=-180
   azang=azang+360*ceil(-azang/360);
   end
if azang >180
   azang=azang-360*floor(azang/360);
   end
%%%

[r0,c0]=size(data);
a1=r0/2;
phi=azang*2*pi/360;
maxl=sqrt(2*((r0/2)^2));
l1=ceil(a1-maxl/2);
u1=l1+maxl-1;
if azang==0
   dataout=data(l1:u1,l1:u1);
   clear data
elseif azang==90
   datao=rot90(data,-1);   %Quick 90 rotation
   clear data
   dataout=datao(l1:u1,l1:u1);
   clear datao
```

```
elseif azang==-90
   datao=rot90(data,1);    %Quick -90 rotation
   clear data
   dataout=datao(l1:u1,l1:u1);
   clear datao
elseif azang==180
   datao=flipud(data)
   clear data
   dataout=datao(l1:u1,l1:u1);
   clear datao
else
   %Interpolation
   for i=1:r0;
      tdata(i,:)=interp(data(i,:),L,E,alpha);
      end
   clear data
   for j=1:L*c0;
      dataic(:,j)=interp(tdata(:,j),L,E,alpha);
      end
   clear tdata
   [r1,c1]=size(dataic);
   datai=dataic(1:(r1-(L-1)),1:(c1-(L-1)));
   clear dataic
   a2=size(datai,1)/2;
   b2=size(datai,2)/2;
   [r2,c2]=size(datai);
   datao=zeros(r2,c2);
   mm=ones(r2,1)*(1:r2);
   i=mm(:);
   mm=mm';
   j=mm(:);
   rad=sqrt((i-a2).^2+(j-b2).^2);
   theta=atan2((j-b2),(i-a2));
   x=round((rad.*cos(theta+phi))+a2);
   y=round((rad.*sin(theta+phi))+b2);
   for ii=1:r2
      im=ii-1;
      for jj=1:c2
        if (x(im*r2+jj)<=r2 & x(im*r2+jj)>=1 & y(im*r2+jj)<=c2 & y(im*r2+jj)>=1)
            datao(ii,jj)=datai(x(im*r2+jj),y(im*r2+jj));
            end
         end
      end
   clear datai
```

```
% Cut image down to size
   [r3,c3]=size(datao);
   a3=size(datao,1)/2;
   b3=size(datao,2)/2;
   maxli=sqrt(2*((r3/2)^2));
   l2=ceil(a3-maxli/2);
   u2=l2+maxli-1;
   datac=datao(l2:u2,l2:u2);
   clear datao

%   Decimate
   [r4,c4]=size(datac);
   cent1=a3-l2;
   os=rem(cent1,L);
   dataout=datac(os+1:L:r4,os+1:L:c4);
   clear datac
   end

return
```

A.2 Elevation Angle Correction

```
%% FUNCTION elcorr2.m
% Purpose: Corrects distortion due to elevation angle. Places data into
% the ground plane. In order to get a close approximation to the actual
% value, interpolates image first.
% Calls: MATLABS interp program.
% Specs: Interpolation performed by parameters L, E, and alpha.
%        Raising L and E greatly increase computation time.

function[dataout]=elcorr2(data,elang,L,E,alpha)

r0=size(data,1);
a1=r0/2;
phi=elang*2*pi/360;
dt=cos(phi);
for i=1:r0;
   tdata(i,:)=interp(data(i,:),L,E,alpha);
   end
clear data
c1=size(tdata,2);
datai=tdata(:,1:(c1-(L-1)));
clear tdata
c2=size(datai,2);
```

```
a2=c2/2;
xx=(ceil(a2-dt*L*a1):dt*L:floor(a2+dt*L*a1));
dataout=datai(:,round(xx));
return
```

A.3 Detection

A.3.1 Maximum-Minimum Threshold Setting.

```
%% FUNCTION detect2.m
%  Purpose:  Try to detect targets using thresholding effect.
%  Calls:
%  Specs:  thresh is a percent value (.0 to 1.0) of the set threshold


function[poss_targs]=detect2(data,thresh)

data=abs(data);
maxpix=max(max(data));
minpix=min(min(data));
range=maxpix-minpix;
tval=thresh.*range+minpix;
[ii,jj]=find(data>=tval);
poss_targs=[ii jj];
return
```

A.3.2 Standard Deviations Above Mean Setting.

```
%% FUNCTION detect3.m
%  Purpose:  Try to detect targets using standard-dev. thresholding effect.
%  Calls:
%  Specs:  thresh is the number of std. deviations above the mean to
%          threshold at.


function[poss_targs]=detect3(data,thresh)

data=abs(data);
data_mean=mean(data(:));
data_std=std(data(:));
tval=thresh.*data_std+data_mean;
[ii,jj]=find(data>=tval);
poss_targs=[ii jj];
return
```

Bibliography

1. Chaney, Ronald D. et al, "Coherent Aspect-Dependent SAR Image Formation." Presented at SPIE Conference on Algorithms for Synthetic Aperture Radar, Orlando, FL, April 1994.
2. Klein, Jeffrey D. "Calibration of Complex Polarimetric SAR Imagery Using Backscatter Correlations," *IEEE Transactions on Aerospace and Electronic Systems*, *AES-28*(2):183–193 (January 1992).
3. Knurr, Kurt W. *Processing of Wide-Angle Synthetic Aperture Radar Signals for Target Detection*. MS thesis, Air Force Institute of Technology (AU), December 1993.
4. Kreithen, Daniel E., et al. "Discriminating Targets from Clutter," *The Lincoln Labratory Journal*, *6*(1):25–52 (1993).
5. Minkler, G. and J. Minkler. *The Principles of Automatic Radar Detection In Clutter*. Baltimore, MD: Magellan Book Company, 1990.
6. Novak, Leslie M., et al. "Studies of Target Detection Algorithms That Use Polarimetric Radar Data," *IEEE Transactions on Aerospace and Electronic Systems*, *AES-25*(2):150–165 (March 1989).
7. Novak, Leslie M., et al. "Performance of a High-Resolution Polarimetric SAR Automatic Target Recognition System," *The Lincoln Labratory Journal*, *6*(1):11–24 (1993).
8. Novak, Leslie M. and Michael C. Burl. "Optimal Speckle Reduction in Polarimetric SAR Imagery," *IEEE Transactions on Aerospace and Electronic Systems*, *AES-26*(2):293–305 (March 1990).
9. Novak, Leslie M. and C. M. Netishen. "Polarimetric Synthetic Aperture Radar Imaging," *International Jounral of Imaging and Systems and Technology*, *4*:306–318 (July 1992).
10. Sacchini, Joséph J. *Development of Two-Dimensional Parametric Radar Signal Modeling and Estimation Techniques with Application to Target Identification*. PhD dissertation, The Ohio State University, 1992.
11. Scharf, Louis L. *Statistical Signal Processing: Detection, Estimation, and Time Series Analysis*. Reading, Massachusetts: Addison-Wesley, 1991.
12. Skolnik, M. I. *Introduction to Radar Systems*. New York: McGraw-Hill, 1980.

Vita

Richard Sumner was born on 18 March, 1970 in Tuscaloosa, Alabama. He graduated from Wilcox Academy in Camden, Alabama in 1988. While attending the University of Alabama he joined the Air Force ROTC, and graduated with honors in May, 1993 with a Bachelor of Science in Electrical Engineering. Upon graduation he received a reserve commission in the USAF as a distinguished ROTC graduate. He was immediately accepted into the Masters Degree program in the School of Engineering, Air Force Institute of Technology.

Permanent address: 31 Willmore Drive
Camden, AL 36726

REPORT DOCUMENTATION PAGE

Form Approved
OMB No. 0704-0188

Public reporting burden for this collection of information is estimated to average 1 hour per response, including the time for reviewing instructions, searching existing data sources, gathering and maintaining the data needed, and completing and reviewing the collection of information. Send comments regarding this burden estimate or any other aspect of this collection of information, including suggestions for reducing this burden, to Washington Headquarters Services, Directorate for Information Operations and Reports, 1215 Jefferson Davis Highway, Suite 1204, Arlington, VA 22202-4302, and to the Office of Management and Budget, Paperwork Reduction Project (0704-0188), Washington, DC 20503.

1. AGENCY USE ONLY (Leave blank)	2. REPORT DATE	3. REPORT TYPE AND DATES COVERED
	December 1994	Master's Thesis

4. TITLE AND SUBTITLE
Processing of Wide-Angle Synthetic Aperture Radar Signals for Detection of Obscured Ground Targets

5. FUNDING NUMBERS

6. AUTHOR(S)
Richard J. Sumner

7. PERFORMING ORGANIZATION NAME(S) AND ADDRESS(ES)
Air Force Institute of Technology, WPAFB OH 45433-6583

8. PERFORMING ORGANIZATION REPORT NUMBER
AFIT/GE/ENG/94D-28

9. SPONSORING/MONITORING AGENCY NAME(S) AND ADDRESS(ES)
Dr Ed Zelnio
WL/AARA
WPAFB OH 45433-6583

10. SPONSORING/MONITORING AGENCY REPORT NUMBER

11. SUPPLEMENTARY NOTES

12a. DISTRIBUTION/AVAILABILITY STATEMENT
Distribution Unlimited

12b. DISTRIBUTION CODE

13. ABSTRACT (Maximum 200 words)

Abstract

This thesis investigates advanced processing techniques for the detection of radar targets in the presence of clutter. It is assumed that the radar data available consist of multi-aspect angle, fully polarimetric Synthetic Aperture Radar (SAR) images. Various techniques are introduced and tested on available SAR data. These techniques attempt to exploit the multi-aspect angles in order to extract target characteristics not available in any single image. SAR images are manipulated in such a way to decrease the probability of false alarms in the target detection process. Target detection performance of the techniques is presented and compared. The techniques are shown to give superior results than that of regular SAR.

14. SUBJECT TERMS	15. NUMBER OF PAGES
Target Detection, Wide-Angle Synthetic Aperture Radar	78
	16. PRICE CODE

17. SECURITY CLASSIFICATION OF REPORT	18. SECURITY CLASSIFICATION OF THIS PAGE	19. SECURITY CLASSIFICATION OF ABSTRACT	20. LIMITATION OF ABSTRACT
UNCLASSIFIED	UNCLASSIFIED	UNCLASSIFIED	UL